MODEL FOR LIQUID BORON OXIDE DROPLET GASIFICATION IN H/O/C/F COMBUSTION ENVIRONMENTS

Final Report
Contract No. N00014-92-C-0225

Prepared by

R.C. Brown and C.E. Kolb
Center for Environmental and Atmospheric Physics
Aerodyne Research, Inc.
45 Manning Road
Billerica, MA 01821

R.A. Yetter and F.L. Dryer,
Department of Mechanical and Aerospace Engineering
Princeton University
Princeton, NJ 08544

H. Rabitz
Department of Chemistry
Princeton University
Princeton, NJ 08544

Prepared for

Dr. Richard S. Miller
Mechanics Division
Code 432
Office of Naval Research
800 N. Quincy Street
Arlington, VA 22217

October 1993

REPORT DOCUMENTATION PAGE

Form Approved
OMB No. 0704-0188

1. AGENCY USE ONLY (Leave blank)	2. REPORT DATE	3. REPORT TYPE AND DATES COVERED
	November 11, 1993	Final Report 10/1/92-10/30/92

4. TITLE AND SUBTITLE

Model for Liquid Boron Oxide Droplet Gasification in H/O/C/F Combustion Environments

5. FUNDING NUMBERS

6. AUTHOR(S)

R.C. Brown and C.E. Kolb, Aerodyne Research, Inc.
R.A. Yetter, F.L. Dryer and H. Rabitz, Princeton University

7. PERFORMING ORGANIZATION NAME(S) AND ADDRESS(ES)

Aerodyne Research, Inc.
45 Manning Road
Billerica, MA 01821

8. PERFORMING ORGANIZATION REPORT NUMBER

ARI-RR-1045

9. SPONSORING/MONITORING AGENCY NAME(S) AND ADDRESS(ES)

Office of Naval Research
800 Quincy Street
Arlington, VA 22217

10. SPONSORING/MONITORING AGENCY REPORT NUMBER

N00014-92-C-0225

11. SUPPLEMENTARY NOTES

12a. DISTRIBUTION/AVAILABILITY STATEMENT

Distribution unlimited; approval for public release

12b. DISTRIBUTION CODE

13. ABSTRACT (Maximum 200 words)

This report presents a model for the gasification of liquid boron oxide droplet in high temperature H/O/C/F environments. The model includes a detailed gas phase reaction mechanism, multi-component molecular diffusion, and heterogeneous gas-surface reactions. The gas phase reaction mechanism consists of 103 reversible reactions for H/O/C, B/H/O/C and B/H/O/C/F combustion systems. The surface reactions include processes that are first order in gas phase reactants and are thermodynamically competitive with vaporization. Model results are presented that illustrate the effect of variations in droplet diameter, gas phase temperature, composition, and oxygen to fluorine mole ratio. In addition, the model calculations are analyzed with reaction flux and gradient sensitivity analysis to determine the fastest and rate-liminting steps.

Model results for several calculations indicate that the addition of fluorine accelerates the gasification process relative to B/H/O/C systems. The degree of enhancement, however, depends upon the temperature and composition of the surrounding gas and the droplet diameter.

14. SUBJECT TERMS

boron, kinetic model, sensitivity analysis, combustion

15. NUMBER OF PAGES
51

16. PRICE CODE

17. SECURITY CLASSIFICATION OF REPORT	18. SECURITY CLASSIFICATION OF THIS PAGE	19. SECURITY CLASSIFICATION OF ABSTRACT	20. LIMITATION OF ABSTRACT
Unclassified	Unclassified	Unclassified	

Abstract

This report presents a model for the gasification of a liquid boron oxide droplet in high temperature H/O/C/F environments. The model includes a detailed gas phase reaction mechanism, multi-component molecular diffusion, and heterogeneous gas-surface reactions. The gas phase reaction mechanism consists of 103 reversible reactions for H/O/C, B/H/O/C and B/H/O/C/F combustion systems. The surface reactions include processes that are first order in gas phase reactants and thermodynamically competitive with vaporization. Model results are presented that illustrate the effect of variations in droplet diameter, gas phase temperature, composition, and oxygen to fluorine mole ratio. In addition, the model calculations are analyzed with reaction flux and gradient sensitivity analyses to determine the fastest and rate-limiting steps.

Model results for several calculations indicate that the addition of fluorine accelerates the gasification process relative to B/H/O/C systems. The degree of enhancement, however, depends upon the temperature and composition of the surrounding gas and the diameter of the droplet.

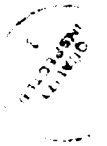

AERODYNE RESEARCH, Inc.

45 Manning Road
Billerica, Massachusetts 01821-3976
(508) 663-9500 Fax (508) 663-4918

November 16, 1993

Defense Technical Information Center
Bldg. 5, Cameron Station
Alexandria, Virginia 22304-6145

Dear Sir,

Enclosed are two copies of our final report "Model for Liquid Boron Oxide Droplet Gasification in H/O/C/F Combustion Environments" on work performed under Contract No. N00014-92-C-0225.

Best Regards,

Robert C Brown

Robert C. Brown
Senior Research Scientist

Enclosures: ARI-RR-1045

RCB/av

Table of Contents

List of Figures

List of Tables

1.0 INTRODUCTION

Elemental boron has long been of interest as an advanced propellant because of its high energy density. Recently, there has been an increased interest in particulate boron oxidation in fluorine enriched environments. This is due, in part, to applications of difluoroamino/nitroamino based oxidizers and new difluoroamino/azido oxetane binders and solid boron in advanced underwater explosives, new propellant formulations and solid propellant ignition systems. The potential advantages of fluorine oxidation include elimination of condensed phase boron oxides and oxyhydrides, as well as faster burn times. Additionally, fluorine has been found to enhance boron's ignition characteristics in oxygen environments by promoting gasification of the ubiquitous oxide layer.

Considering molecular oxygen and molecular fluorine as oxidizers, it is also interesting to note (see Table 1) that the heat of reaction in forming gaseous BF_3 is higher or comparable to the energy released in oxidation to liquid B_2O_3. The latter is difficult to achieve within typical residence times for practical devices because of a kinetic bottleneck in the condensation process of $B_2O_3(g)$ to $B_2O_3(l)$ through formation of the intermediate $HBO_2(g)$.[1,2] In mixtures consisting of both fluorine and oxygen, the equilibrium boron product distribution shifts toward OBF. Energetically, OBF formation is comparable to $B_2O_3(l)$ based on a mass weighting of the fuel only; however, its formation is less desirable when based on the total weights of fuel and oxidizer. Heats of reaction will vary with different fluorinated/oxygenated oxidizers. Because the heat of formation for HF is more exothermic than that for H_2O, the overall heat released from combined B/O/H/C/F based systems will generally be competitive with B/O/H/C based systems.

Table 1. Heats of Oxidation and Fluorination

Reaction	KJ/gm of fuel	KJ/gm of fuel + oxidizer
$B(s) + 3/4O_2(g) \rightarrow 1/2B_2O_3(l)$	58	18
$B(s) + 3/2F_2(g) \rightarrow BF_3(g)$	105	17
$B(s) + 1/2O_2(g) + 1/2F_2(g) \rightarrow OBF(g)$	56	13

The extent to which the thermodynamic potential of boron/fluorine systems is realized ultimately depends on the combustion kinetics. The goal of the present work is to develop a kinetic model for boron combustion that can be used in helping to identify critical parameters and, in conjunction with experimental studies, to better understand combustion mechanisms. Since particulate boron combustion is a complex multistep process involving both heterogeneous and homogeneous chemical kinetics, this is an inherently mutiphased task. Under an earlier project sponsored by the Air Force Office of Scientific Research models were developed for the homogeneous[1-3] and heterogeneous[3-5] kinetics associated with particulate boron in post-hydrocarbon combustion gases. The heterogeneous processes treated included both the high

temperature surface burning of a relatively 'clean' boron particle[4] and chemically facilitated gasification of the boron oxide coating[5]. The overall goal of the present Office of Naval Research effort is to extend the model for B/H/O/C combustion systems to include fluorine chemistry. The specific objectives are to characterize the general mechanistic behavior of these systems, to identify the most important gas-phase reaction pathways and, hence, to determine the reaction rate parameters whose experimental and theoretical evaluation would significantly enhance current predictive capabilities.

Initial work extended the earlier gas-phase oxidation model for B/O/H/C combustion systems[1-3] to include fluorine chemistry[6]. It included a description of a reaction mechanism for high temperature B/H/O/C/F combustion systems, the results of kinetic calculations illustrating the mechanistic behavior of these systems, and an analysis of the dominate reaction fluxes and key reaction pathways. Here we formulate models for the heterogeneous gas-surface kinetics. The study specifically treats the gasification of a liquid boron oxide droplet. However, a preliminary summary of the surface kinetics model for oxidation of a solid boron particle is also reported for completeness. However, the latter model has not been extensively studied and only serves as the starting point for more detailed analysis.

The remainder of this report is organized as follows. Section 2.0 presents an overview of the single particle combustion model and summarizes the governing equations for gasification of a liquid boron oxide droplet. Section 3.0 reviews the gas phase oxidation model. Section 4.0 describes the heterogeneous B_2O_3 gasification kinetics model. Section 5.0 presents model results. Section 6.0 summarizes the work to date and describes further research efforts. All technical references are listed in Section 7.0. Appendix A contains a complete listing of the gas phase oxidation mechanism. Appendix B lists the preliminary heterogeneous (gas-surface) reaction mechanism for solid boron in H/O/C/F combustion environments.

2.0 SPHERICAL PARTICLE COMBUSTION MODEL

2.1 Model Overview

The spherical particle combustion model treats the combustion of a spherical (1-dimensional) particle in a hot quiescent oxidizing environment. The key processes are shown schematically in Figure 1.

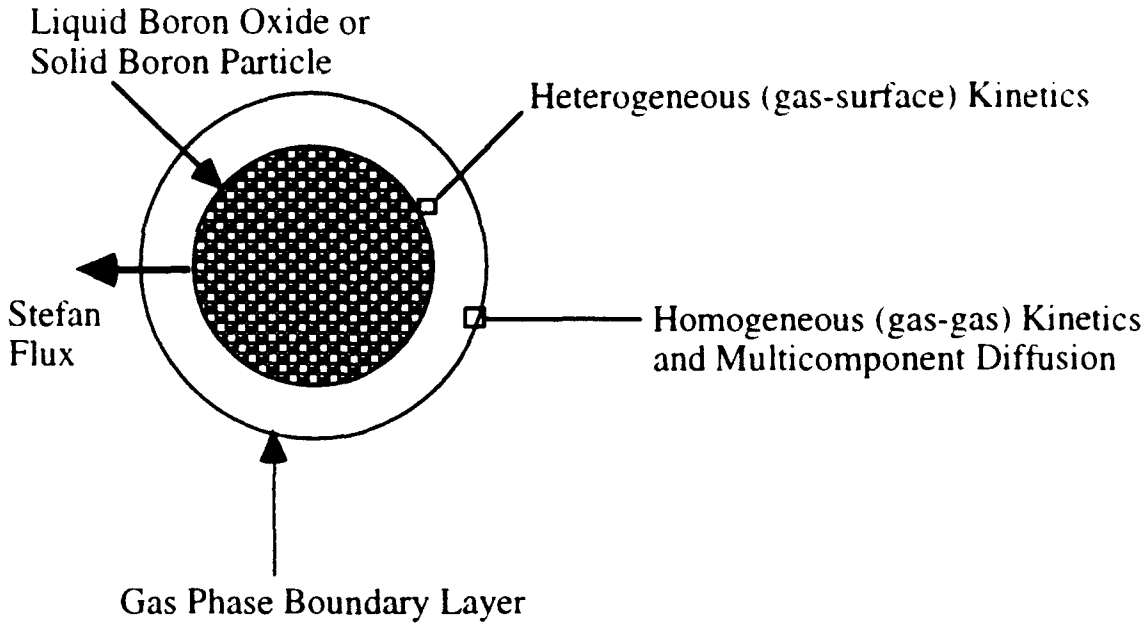

Figure 1. Schematic of Spherical Particle Combustion in Reactive Environments.

The present report summarizes a numerical model and analysis for the chemically facilitated gasification of a liquid boron oxide droplet in a high temperature quiescent environment consisting of post combustion gases containing fluorine. The physical model is that of a liquid boron oxide droplet instantaneously placed in a quiescent high temperature oxidizing environment consisting of equilibrium products of fluorinated derivative of HMX and TMETN binder.[6] The effects of temperature, mixture composition, and droplet diameter on the gasification rate are reported. The numerical model and solution procedure have been described in detail elsewhere[7] and are only briefly described here. The calculations were performed under quasi-steady conditions in which the droplet diameter was held fixed in time and under transient conditions in which the droplet diameter was allowed to regress.

2.2 Governing Equations

The low Mach number gas-phase flow is described as an ideal gas with elementary detailed kinetics and multi-component mass and thermal diffusion. The assumption of isobaric flow applies and the momentum equation is satisfied trivially by the Stefan flow away from the particle surface. The assumptions employed here include: (1) negligible viscous dissipation, (2) no buoyancy effects, (3) no forced convection on the particle, and (4) no Dufour effects. The range of ambient pressures to be studied by the model are limited to those for which the ideal gas equation of state and kinetics are valid. Thus, the boundary separating the condensed-phase from the gas-phase will be treated as a discrete interface.

The equations governing the gas-phase are:

$$\frac{\partial \rho_g}{\partial t} + \frac{1}{r^2}\frac{\partial}{\partial r}(r^2 \rho_g v_g) = 0 \tag{1}$$

$$\rho_g \frac{\partial Y_{gk}}{\partial t} + \frac{1}{r^2}\frac{\partial}{\partial r}(r^2 \rho_g Y_{gk} V_{gk}) - \dot{\omega}_{gk} W_{gk} = 0 \quad (k=1,\ldots,G) \tag{2}$$

$$\rho_g c_{pg} \frac{\partial T_g}{\partial t} + \rho_g c_{pg} v_g \frac{\partial T_g}{\partial r} - \frac{1}{r^2}\frac{\partial}{\partial r}(r^2 \lambda_g \frac{\partial T_g}{\partial r}) + \sum_{k=1}^{G} \rho_g Y_{gk} V_{gk} c_{pgk} \frac{\partial T_g}{\partial r} + \sum_{k=1}^{G} \dot{\omega}_{gk} h_{gk} W_{gk} = 0 \tag{3}$$

$$\rho_g = \frac{p \overline{W}_g}{R T_g} \tag{4}$$

In these equations, r denotes the spatial radial coordinate; t, the time; ρ_g, the mass density of the gas-phase; v_g, the radial velocity of the gas-phase; Y_{gk}, the mass fraction of the kth gas-

phase species; V_{gk}, the diffusion velocity of the kth gas-phase species; $\dot{\omega}_{gk}$, the molar production rate by chemical reaction of the kth gas-phase species per unit volume; W_{gk}, the molecular weight of the kth gas-phase species; $\overline{W}_g$ the mean molecular weight of the gas-phase mixture; c_{pg}, the constant pressure heat capacity of the gas-phase mixture; c_{pgk}, the constant pressure heat capacity of the kth gas-phase species; T_g, the gas-phase temperature; λ_g, the thermal conductivity of the gas-phase mixture; h_{gk}, the specific enthalpy of the kth gas-phase species; p, the pressure; R, the universal gas constant; and G, the number of gas-phase species.

The interfacial conditions at the liquid-phase/gas-phase boundary (lg) for $t \geq 0$ are:

$$r = r_{lg} \tag{5}$$

$$T_l = T_g \tag{6}$$

$$\dot{\omega}_{lgk} + \overline{\omega}_{lgk} = \rho_g Y_{gk}(v_g + V_{gk}), \quad (k=1,\ldots\ldots,G) \tag{7}$$

$$\sum_{k=1}^{G} \left(\dot{\omega}_{lgk} + \overline{\omega}_{lgk}\right) = \rho_g v_g \tag{8}$$

$$\lambda_g \frac{\partial T_g}{\partial r} = \lambda_l \frac{\partial T_l}{\partial r} + \sum_{k=1}^{G+LG} \left(\dot{\omega}_{lgk} h_k + \overline{\omega}_{lgk} \overline{h}_k\right) \tag{9}$$

In these equations, the elements of $\overline{\omega}_k$ include both the processes of vaporization and condensation and of solution and dissolution. Hence, $\overline{h}_k$ includes both the enthalpies of solution and the heats of vaporization.

The outer boundary condition for $t \geq 0$ is:

$$r \rightarrow \infty \tag{10}$$

$$\lim_{r \rightarrow \infty} Y_{gk} = Y_{gk\infty}, \quad (k=1,\ldots\ldots,G) \tag{11}$$

$$\lim_{r \rightarrow \infty} T_g = T_{g\infty} \tag{12}$$

The initial conditions for the gas and liquid/gas interface are:

$$r_{lg} < r < \infty, \qquad [T_g]_{t=0} = T_{g0}, \quad [Y_{gk}]_{t=0} = Y_{gk0}, \ (k=1,\ldots\ldots,G) \tag{13}$$

$$0 < r < r_{lg}, \qquad [T_l]_{t=0} = T_{l0} \tag{14}$$

$$r = r_{lg}, \qquad [C_{lgk}]_{t=0} = C_{lgk0}, \ (k=1.....LG) \tag{15}$$

In these equations, C_{lgk} denotes the number per unit surface area of the kth surface complex at the liquid/gas interface.

3.0 GAS PHASE KINETICS

This section briefly reviews the model being used to treat the gas phase kinetics. More complete discussions are given in References[1-3] for B/H/O/C systems and in Reference[6] for B/H/O/C/F systems.

3.1 Gas Phase Reactants

The reactants included in the gas phase oxidation model are listed in Table 2. They include the dominant speciation in post-hydrocarbon combustion environments (H/O/C), boron oxides and oxyhydrides that are important intermediates and products in boron assisted hydrocarbon combustion (B/H/O/C), and the additional boron fluorides and oxyfluorides that arise when fluorine is included in the system (B/H/O/C/F).

Table 2. B/H/O/C/F Gas Phase Species List*

H/O/C	B/H/O/C	B/H/O/C/F
H	B	F
O	BO	HF
OH	BO_2	BF
H_2O	B_2O_2	BF_2
H_2	B_2O_3	BF_3
O_2	HBO	OBF
CO	HOBO	
CO_2		
HO_2		
H_2O_2		
HCO		

* HO_2, H_2O_2 and HCO are used only in describing H/O/C chemistry.

The reactant list in Table 2 is not intended to suggest that these will be the only species of importance for an arbitrary propellant formulation. Rather, these reactants were selected based on equilibrium analyses of specific propellant formulations and a given range of combustion temperature and pressure. The boron containing species in Table 2 were typically found to be dominant (largest equilibrium mole fraction) for the temperatures of interest and for a range of boron to oxidizer mass ratios. Notable species which are not included are the oxide B_2O, the HBO isomer HOB and boron hydrides BH and BH_2. Additionally, the species HO2, H_2O_2 and HCO are treated only within the kinetic mechanism for H/O/C systems. Reactions between these species and boron species have not been included. An expanded gas phase model for B/H/O/C systems which includes HCO reactions, as well as HOB and boron hydride has been reported by Pasternak.[8]

Heats of formation and entropies for gas phase species are listed in Table 3. The heat of formation for HBO is from Page[9]. Similar values have been reported by other workers.[10] The heat of formation for HO_2 is from Hills and Howard[11]. Thermochemical constants for the remaining species are from the JANNAF Tables[12].

Table 3. B/O/H/C/F Thermochemical Parameters*

Species	$\Delta H_{f,298}$	S_{298}	Cp,300	Cp,500	Cp,800	Cp,1000	Cp,1500
H	52.10	27.39	4.97	4.97	4.97	4.97	4.97
O	59.56	38.47	5.23	5.08	5.02	5.00	4.98
OH	9.32	43.88	7.15	7.07	7.13	7.33	7.87
H_2	.00	31.21	6.90	7.00	7.07	7.21	7.73
O_2	.00	49.01	7.01	7.44	8.07	8.35	8.72
H_2O	-57.80	45.10	8.00	8.44	9.22	9.87	11.26
HO_2	3.50	54.43	8.36	9.48	10.75	11.37	12.34
H_2O_2	-32.53	55.66	10.41	12.34	14.29	15.21	16.85
CO	-26.42	47.21	6.95	7.14	7.61	7.95	8.41
CO_2	-94.06	51.08	8.91	10.65	12.32	12.99	13.93
HCO	10.40	53.66	8.24	9.28	10.74	11.52	12.56
B	133.80	36.65	4.97	4.97	4.97	4.97	4.97
BO	.00	48.60	7.00	7.39	7.86	8.11	8.53
BO_2	-68.00	54.90	2.54	13.05	13.64	13.94	14.43
B_2O_2	-108.99	57.96	15.79	16.80	18.00	18.61	19.65
B_2O_3	-199.80	67.80	19.19	20.52	22.09	22.90	24.26
HBO	-60.00	48.40	9.38	10.42	11.66	12.31	13.42
HBO_2	-133.99	57.27	11.95	13.34	15.01	15.89	17.47
F	18.86	37.92	5.25	5.19	5.12	5.08	5.02
BF	-27.70	47.89	7.65	7.93	8.28	8.46	8.77
BF_2	-141.00	59.05	11.73	12.21	12.76	13.03	13.48
BF_3	-271.42	60.77	15.65	16.54	17.59	18.12	18.99
OBF	-143.99	53.70	11.69	12.34	13.12	13.51	14.18
HF	-65.14	41.51	6.36	6.62	6.98	7.20	7.67
N_2	.00	45.77	6.95	7.08	7.50	7.83	8.32

*units are Kcal/mol for $\Delta H_{f,298}$ and cal/mol-K for S and C_p

The heats of formation in Table 3 were used to compute the gas phase bond energies listed in Table 4. These are later used in estimating adsorption enthalpies for the gas phase reactants in Table 2 on boron oxide surfaces.

Table 4. Gas Phase Bond Strengths

Bond	Bond Order	Bond Strength	
		(ev)	(Kcal/mol)
F-H	1	5.91	136.2
F-B	1	7.83	180.5
F-BF	1	5.59	132.3
F-BF_2	1	6.62	149.4
F-BO	1	7.06	163.0
HB=O	2	9.23	225.4
B=O	2	8.37	193.4
OBB=O	2	8.29	193.4
FB=O	2	7.62	175.8
HOB=O	2	7.51	173.6
OBOB=O	2	7.40	171.0
OB=O	1.5	5.51	127.6
OB-BO	1	4.73	109.0
HO-BO	1	6.22	143.3
OBO-BO	1	5.75	131.8
BO-B	1	4.80	110.8
H-BO	1	4.28	112.1
H-BH	1	4.77	109.9
H-B	1	3.48	80.1
H-O	1	4.38	102.3
H-OH	1	5.12	119.2
h-OBO	1	5.00	118.1
C=O	2	11.11	256.0
OC=O	2	5.54	127.6

3.2 Gas Phase Reaction Mechanism

A complete listing of gas phase reaction mechanism is given in Appendix A. The tabulated reaction enthalpies were computed from reactant and product heats of formation using the data listed in Table 3. The reaction mechanism is limited to bimolecular and termolecular (three body) reactions. Higher order reactions such as A + B + C = D + E were neglected. Additionally, reaction channels resulting in products not listed in Table 2, e.g. boron hydrides, are excluded to ensure consistency.

The portion of reaction mechanism describing the chemistry involving H/O/C species has been extensively used with good results to describe the kinetics of $CO/H_2/O_2$ mixtures.[13] Rate parameters for the reactions involving boron containing species are highly uncertain. To date, relevant laboratory studies have been limited to reactions between atomic B or BO with O_2, CO_2 and H_2O[14-20] and to reactions between BF and he oxidants O_2, O and NO_2.[21,22] Rate parameters for the remaining reactions have been estimated. For many of the boron fluoride and oxyfluoride reactions, initial estimates were obtained from a propellant afterburning study[23]. The remainder were estimated using simple scaling relationships based on the ratios of translational, rotational, and vibrational partition functions.

3.3 Mechanistic Behavior

An example of the homogeneous, constant pressure, adiabatic kinetics of a B/O/H/C/F mixture is shown in Figure 2. Only the boron-containing species are given. The results show OBF to be the dominant boron species. The mole fractions of HBO_2 and B_2O_3 were typically less than 0.02. Note that the temperature rise is associated with OBF formation and that all the other boron-containing species appear to simultaneously form OBF. The rate of OBF formation was found to be equal to or faster than HBO_2 and B_2O_3 formation in mixtures without fluorine.[1,2] These results are typical of those found for mixtures with an oxygen/fluorine mole ratio near unity. A more extensive analysis of model results for the gas phase chemistry is given in Reference 6.

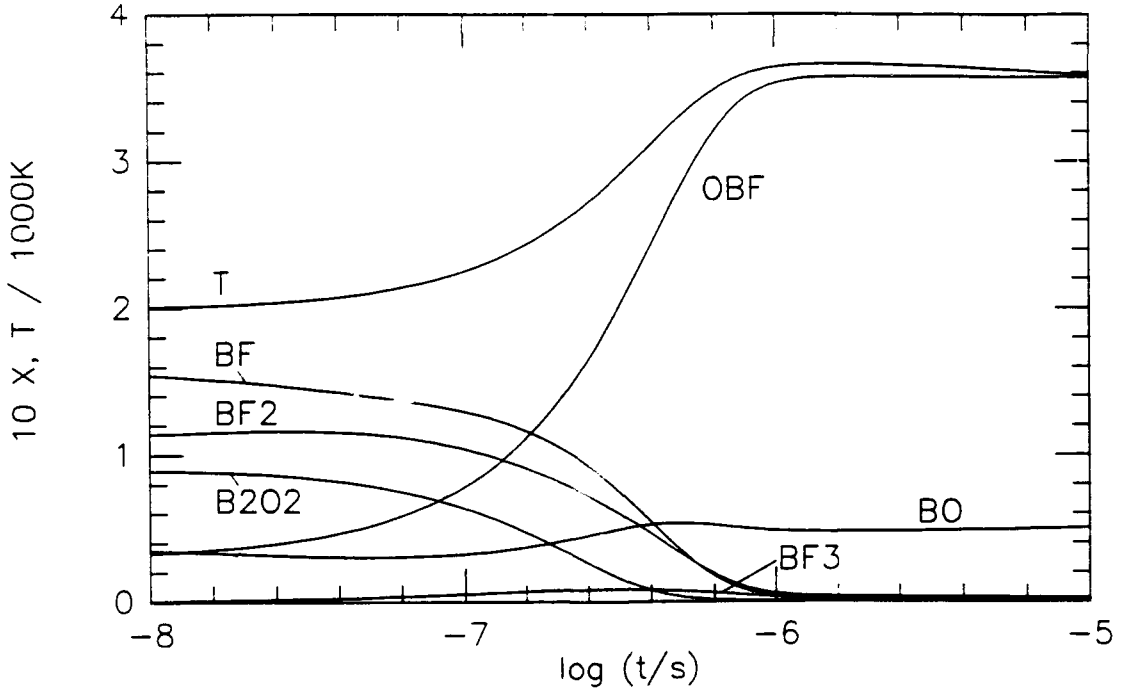

Figure 2. Boron species and temperature profiles for an adiabatic, constant pressure (1 atm) homogeneous system with an initial temperature of 2000 K. The initial mixture consisted of $X(BF)=0.16$, $X(BF_2)=0.11$, $X(BO)=0.04$, $X(B_2O_2)=0.09$, $X(OBF)=0.03$, $X(CO)=0.04$, $X(H_2)=0.04$, $X(O_2)=X(H_2O)=X(HF)=X(N_2)=0.13$.

3.4 Critical Gas Phase Reactions

The most sensitive reactions are reported in Table 5. Most of these reactions are associated with oxidation of initial reactants to OBF. A few are associated with the relatively minor sequence of BF conversion to BF_2 and BF_3, which was found to be significant only for O/F ratios much less than one. The simultaneous formation of OBF by boron fluorides, boron oxides, and boron oxyhydrides is in contrast to the sequential formation of B_2O_3 found in systems without fluorine, i.e., BO ---> BO_2 ---> HBO_2 ---> B_2O_3. It is important to note that the reactions designated as most sensitive in Table 5 specifically refers to systems with both oxygen and fluorine. When fluorine is absent the critical reactions differ from those in Table 5. In this case the earlier results reported in References 1-3 are more applicable.

Table 5. Most Sensitive Gas Phase Reactions for B/H/O/C/F Systems

B/H/O/C/F Reactions	$F + H_2 = HF + H$
	$F + H_2O + OH + HF$
	$F + B_2O_2 = OBF + BO$
	$F + HBO = OBF + H$
	$F + HBO_2 = OBF + OH$
	$BF + O = BO + F$
	$BF + OH = OBF + H$
	$BF + O_2 = OBF + O$
	$BF + BO_2 = OBF + BO$
	$BF_2 + O = OBF + F$
	$BF_2 + H = BF + HF$
	$BF_2 + BO = OBF + BF$
	$BF_2 + HF = BF_3 + H$
	$BF_2 + BF_2 = BF_3 + BF$
	$BF_3 + BO = BF_2 + OBF$
B/H/O/C Reactions	$BO + O_2 = BO_2 + O$
	$BO + H_2 = HBO + H$
	$BO + HBO_2 = B_2O_3 + H$
	$B_2O_2 + H = BO + HBO$
	$B_2O_2 + O = BO + BO_2$
	$B_2O_2 + OH = BO + HBO_2$
	$HBO + OH = BO + H_2O$
	$HBO + OH = HBO_2 + H$
H/O/C Reactions	$H + O_2 = O + OH$
	$O + H_2 = H + OH$

4.0 $B_2O_3(l)$ SURFACE REACTIONS

A detailed description of the model for boron oxide gasification in B/H/O/C combustion systems has been presented elsewhere [5]. Here, that model is extended to include reactants containing fluorine.

4.1 Global Reactions

Global surface reactions involving gas phase reactants containing fluorine were selected using the three criteria used in earlier work.[5] The selection criteria are:

(1) reactions first order in gas phase reactants
(2) reactions whose reaction enthalpy is less than 110 Kcal/mol
(3) reactions yielding gas phase products which are consistent with the gas phase oxidation model.

Based on these criteria, four additional reactions were identified. They are listed in Table 6 along with three reactions previously used in modeling $B_2O_3(l)$ gasification in B/H/O/C combustion environments.

Table 6. Global Reactions: $B_2O_3(l) + Z(g)$ = products

Reaction	$\Delta H_{r,298}$ (Kcal/mol)
R_1 $B_2O_3(l) + O(g) = BO_2(g) + BO_2(g)$	104.2
R_2 $B_2O_3(l) + OH(g) = BO_2(g) + HOBO(g)$	88.3
R_3 $B_2O_3(l) + H_2O(g) = HOBO(g) + HOBO(g)$	89.4
R_4 $B_2O_3(l) + F(g) = BO_2(g) + OBF(g)$	68.6
R_5 $B_2O_3(l) + F(g) \rightarrow BO(g) + OBF(g) + O(g)$	96.2
R_6 $B_2O_3(l) + HF(g) = HOBO(g) + OBF(g)$	86.7
R_6 $B_2O_3(l) + BF(g) = B_2O_2(g) + OBF(g)$	74.3

Reactions R_4 and R_5 are the isoelectronic analogs of reactions R_2 and R_3. Isoelectronic analogs of reaction R_6.

$$B_2O_3(l) + HBO(g) = B_2O_2(g) + HOBO \qquad \Delta H_r = 116.6 \qquad (16)$$

$$B_2O_3(l) + CO(g) = B_2O_2(g) + CO_2(g) \qquad \Delta H_r = 123.0 \qquad (17)$$

are not included because their reaction enthalpies exceeded 110 Kcal/mol. The model treats each of the reactions in Table 6 as reversible. The discussion that follows describes adsorption and desorption reaction steps for these reactions in the forward direction. The backward reactions are treated by taking each 'elementary' reaction step to be reversible. A consequence of this is that the model will include both first-order (with respect to surface complexes) and second-order desorption processes.

4.2 Elementary Reaction Mechanism

4.2.1 First Order Adsorption and Desorption Channels

The global reactions in Table 6 have been represented by simple adsorption and desorption reaction steps using the same model previously used to treat B/H/O/C systems. This consists of following steps.

Step (1)

The B_2O_3 surface is taken to consist of chains of BO_3 units and reactive surface sites are represented by:

$$^{O}{>}B\text{-}O\text{-}B{<}_{O} \qquad (18)$$

Step (2)

Adsorption of a gas phase species X-Y is taken to occur via bonding between the more electronegative component (Y) to boron. Depending on the specific reactant, the more electropositive component (X) may bond to oxygen.

$$^{O}{>}B\text{-}O\text{-}B{<}_{O} + XY \longrightarrow {}^{O}{>}B\text{-}O\text{-}\overset{\displaystyle X\text{---}Y}{\overset{\displaystyle |\quad |}{B}}{<}_{O} \qquad (19)$$

or

$$^{O}{>}B\text{-}O\text{-}B{<}_{O} + XY \longrightarrow {}^{O}{>}B\text{-}O\text{-}\overset{\displaystyle Y\text{-}X}{\overset{\displaystyle |}{B}}{<}_{O} \qquad (20)$$

We also allow the -O--B< and X--Y bonds to be broken during adsorption resulting in two surface species:

$$O_{>B\text{-}O\text{---}B<O} \begin{matrix} X\text{---}Y \\ | \quad | \end{matrix} \text{-----} > O_{>B\text{-}O\text{-}X} + O_{>B\text{-}Y} \qquad (21)$$

One exception to the above description is when X is boron (e.g. BF). In this case, the boron atom is taken to be inserted in the >B-O bond to give >B-B=O. This is the least endothermic bonding configuration and is also consistent with $B_2O_2(g)$ as a gas phase product (Reaction R6).

Step (3)

Based on step (2), all adsorption products have the form $O_{>B\text{-}Z}$. Desorption is then taken to occur by breaking two B-O bonds and forming a B=O double bond. After extending the BO_3 chain for clarity, bond cleavage and formation during desorption consists of the following:

surface species bond cleavage bond formation

$$\begin{matrix} O_{>BO} \\ >B\text{-}Z \\ O_{>BO} \end{matrix} \text{ ---> } O_{>B.} + .O\text{-}B<_{O} + O\text{-}B\text{-}Z \text{ ---> } O_{>B\text{-}O\text{-}B<O} + O{=}BZ \qquad (22)$$

For simplicity, the process will be represented as $O_{>B\text{-}Z}$ ---> O=B-Z. Based on steps (2) and (3), adsorption of gas phase reactant X-Y yields two surface species. The subsequent desorption of both complexes removes one B_2O_3 molecule from the surface.

The above description is not presented as a postulated mechanism for the surface reactions in Table 6. Rather, given our assumptions concerning the B_2O_3 surface structure, this model gives a simple description of bond formation and cleavage required to yield gas phase products which are consistent with the global reactions in Table 6. To illustrate this, the complete reaction sequence for each reaction in Table 6 is given in Table 7 in terms of the adsorption and desorption reaction steps.

Table 7. Model Reaction Sequence for $B_2O_3(l)$ Surface Reactions

ID	Reactants	Adsorption Products	Desorption Products
R1	^{O}>B-O-B<$_{O}$ + O ---> O | ^{O}>B-O--B<$_{O}$ --->	^{O}>B-O. + ^{O}>B-O. --->	O=BO + O=BO
R2	^{O}>B-O-B<$_{O}$ + OH ---> OH | ^{O}>B-O--B<$_{O}$ --->	^{O}>B-OH + ^{O}>B-O. --->	O=BOH + O=BO
R3	^{O}>B-O-B<$_{O}$ + H_2O ---> H--OH | | ^{O}>B-O--B<$_{O}$ --->	^{O}>B-OH + ^{O}>B-OH --->	2 O=BOH
R4	^{O}>B-O-B<$_{O}$ + F ---> F | ^{O}>B-O--B<$_{O}$ --->	^{O}>B-O. + ^{O}>B-F --->	O=BO + O=BF
R5	^{O}>B-O-B<$_{O}$ + HF ---> H--F | | ^{O}>B-O--B<$_{O}$ --->	^{O}>B-OH + ^{O}>B-F --->	O=B-OH + O=BF
R6	^{O}>B-O-B<$_{O}$ + BF ---> B----F | | ^{O}>B-O--B<$_{O}$ --->	^{O}>B-BO + ^{O}>B-F --->	O=B-B=O + O=BF

To estimate adsorption enthalpies, bond energies for surface speciation have been estimated using the gas phase bond energies in Table 4. These bond energies are listed in Table 8 along with the gas phase bond energies for species with similar configurations. For D_3 we have adopted the gas phase O-H bond strength in HOBO. For >BB=O we have used the B=O bond strength in B_2O_2. For the remaining complexes, the gas phase bond energies have been adjusted to reflect differences in boron's hybridization. One difference between the surface complexes and gas phase species for D_2, D_4, D_5 an D_7 is the boron- oxygen double bond in the gas phase species (i.e. O=B-Z) versus the two boron-oxygen single bonds for the complex (i.e. ^{O}>B-Z). Consequently, in these cases the bond energies for surface complexes have been set equal to the gas phase bond energies minus 10 Kcal/mol.

Table 8. $B_2O_3(l)$ Surface Species Bond Strengths

Surface Complex Bond	Bond Strength (eV)	Bond Strength (Kcal/mol)	Gas Phase Bond	Bond Strength (Kcal/mol)
D_1 $O_>$BO-B<	5.75	110.0		
D_2 $O_>$B-F	6.95	153.0	OB-F	163.0
D_3 $O_>$BO-H	5.00	118.1	OBO-H	118.1
D_4 $O_>$B-OH	6.22	133.3	OB-OH	143.3
D_5 $O_>$B-BO	4.73	100.0	OB-BO	109.0
D_6 $O_>$BB=O	8.29	191.0	OBB=O	193.4
D_7 $O_>$B-O.	5.51	117.0	OB-O	127.0

Adsorption enthalpies and rate parameters for adsorption reactions are listed in Table 9. For the adsorption rates we have assumed a rate constant given by

$$k_a = k_0 \sqrt{T} s_0 e^{\left(-\frac{E_a}{RT}\right)} \tag{23}$$

where

$$k_0 = \sqrt{\frac{K_B \pi m}{2}} \tag{24}$$

In Equation (23), E_a is the adsorption activation energy and s_0 is the probability that a molecule hitting the surface adsorbs. Rate parameters for adsorption of O(g), OH(g) and H_2O(g) were estimated previously and are used here without any change. Anderson reports that his preliminary results indicate the HF and H_2O exhibit about the same reactivity with respect to B_2O_3 clusters.[24] Consequently, H_2O adsorption rate parameters have been adopted to describe HF adsorption. Similarly, we will also assume that F(g) has the same rate parameters as OH(g).

Table 9. First-order Adsorption Rate Parameters for $B_2O_3(l)$ Surface

Adsorption Reaction $B_2O_3(l) + Z(g)$ ---> adsorption products	$k_a = k_0\sqrt{T}s_0e^{\left(\frac{-E_a}{RT}\right)}$			
	$\Delta H_{f,298}$ (Kcal/mol)	k_0 (cm/s)	s_0	E_a (Kcal/mol)
S-1 >B-O-B< + O = >B-O. + >B-O.	-17	910.	0.1	0.00
S-2 >B-O-B< + OH = >B-O. + >B-OH	-33	882.	0.1	0.00
S-3 >B-O-B< + H_2O = >B-OH + >B-OH	-32	857.	0.05	10.0
S-4 >B-O-B< + F = >B-O. + >B-F	-50	834.	0.1	0.00
S-5 >B-O-B< + HF = >B-OH + >B-F	-32	813.	0.05	10.0
S-6 >B-O-B< + BF = >B-BO + >B-F	-59	666.	0.01	30.0

Desorption enthalpies are estimated using the product heats of formation Table 3 and the adsorption enthalpies from Table 9. As an example, consider reactions R1-R3 in Table 2, i.e.

$$^{O}{>}B\text{-}O\text{-}B{<}_{O} + O \;\text{---}> {}^{O}{>}B\text{-}O. + {}^{O}{>}B\text{-}O. \;\text{---}> BO_2 + BO_2 \qquad (25)$$

$$^{O}{>}B\text{-}O\text{-}B{<}_{O} + OH \;\text{---}> {}^{O}{>}B\text{-}OH + {}^{O}{>}B\text{-}O. \;\text{---}> BO_2 + HOBO \qquad (26)$$

$$^{O}{>}B\text{-}O\text{-}B{<}_{O} + H_2O \;\text{---}> {}^{O}{>}B\text{-}OH + {}^{O}{>}B\text{-}OH \;\text{---}> HOBO + HOBO \qquad (27)$$

From (9), the desorption enthalpy for >B-O. is 1/2[H_1-H_a(O)] where H1 is the reaction enthalpy for the global reaction R1 and Ha(O) is the adsorption reaction for O(g). Similarly, the desorption enthalpy for >B-OH using (11) is 1/2[H_3-$H_a(H_2O)$]. As a consistency check, the sum of the desorption enthalpies for >B-O. and >B-OH should be close to H_2-H_a(OH). A similar procedure is used to estimate the desorption enthalpies for >B-F and >B-BO.

First order desorption rates are taken to have the form,

$$k_1 = A_1 \times \exp(-E_1/kT) \qquad (28)$$

The desorption coefficients A_1 are given approximately by the transition state frequency factor k_BT/h. As a first approximation, the desorption activation energies are taken to equal the

desorption enthalpies. A summary of desorption enthalpies and rate parameters are given in Table 10. The result of these estimations is that the desorption rates for the complexes >B-Z are largely independent of Z whereas, from Table 8, adsorption rates are dependent on the gas phase reactant.

Table 10. First-order Desorption Rate Parameters for $B_2O_3(l)$ Surface

Desorption Reaction	Forward Rate Parameters $k_1 = A_1 \exp(-E_1/RT)$		
	ΔH_1 (Kcal/mol)	A_1 (ps^{-1})	E_1 (Kcal/mol)
S-7 $O_{>}B\text{-}O = O\text{=}B\text{-}O$	55.6	0.02 x T	55.6
S-8 $O_{>}B\text{-}OH = O\text{=}B\text{-}OH$	55.7	0.02 x T	55.7
S-9 $O_{>}B\text{-}F = O\text{=}B\text{-}F$	56.0	0.02 x T	56.0
S-10 $O_{>}B\text{-}BO = O\text{=}B\text{-}BO$	57.3	0.02 x T	57.3

4.2.2 Reversibility

It is necessary to ensure that the reactions describe above are reversible. For the global reactions in Table 2 to be reversible, the adsorption reactions in Table 7 will also be considered reversible. Thus the model also includes the second-order desorption reactions listed in Table 11. Here again, we have taken a simple Arrhenius rate.

Table 11. Second-order Desorption Rate Parameters for $B_2O_3(l)$ Surface

No.	Desorption Reaction	Forward Rate Parameters $k_2 = A_2 \exp(-E_2/RT)$	
		A_2 (cm^2/complex-s)	E_2 (Kcal/mol)
S-11	$O_{>}B\text{-}O + O_{>}B\text{-}O = B_2O_3(l) + O(g)$	3.0×10^{-5}	5.
S-12	$O_{>}B\text{-}OH + O_{>}B\text{-}O = B_2O_3(l) + OH(g)$	3.0×10^{-5}	5.
S-13	$O_{>}B\text{-}OH + O_{>}B\text{-}OH = B_2O_3(l) + H_2O(g)$	3.0×10^{-5}	10.
S-14	$O_{>}B\text{-}F + O_{>}B\text{-}OH = B_2O_3(l) + F(g)$	3.0×10^{-5}	5.
S-15	$O_{>}B\text{-}F + O_{>}B\text{-}OH = B_2O_3(l) + HF(g)$	3.0×10^{-5}	10.
S-16	$O_{>}B\text{-}F + O_{>}B\text{-}BO = B_2O_3(l) + BF(g)$	3.0×10^{-5}	10.

From Table 2, the primary gas phase reactants are O, OH, H_2O, F, HF and BF. The subsequent gas phase products are BO_2, HOBO, OBF and B_2O_2. Thus, there are no reactions between these products and the B_2O_3 surface which satisfy the three selection criteria. Therefore, to ensure reversibility, we will assume that adsorption of these products to yield the original surface complex is the only viable channel, i.e. HOBO adsorbs to yield a >B-OH complex, B_2O_2

adsorbs to yield a >B-BO complex, etc. Rate parameters for these additional adsorption reactions where expressed in terms of the equilibrium constant K_p and rate constants for the adsorption reactions in Table 9. The explicit forms for these rates are given in Table 12.

Table 12. First-order Adsorption Rate Parameters for B_2O_3(l) Surface

No.	Reaction	k3
S-17	BO_2(g) ---> ^{O}>B-O	$\frac{k_{s-7}}{K_p(BO_2)}\sqrt{\frac{k_{s-1}K_p(O)RT}{k_{s-11}}}$
S-18	HBO_2(g) ---> ^{O}>B-OH	$\frac{k_{s-8}}{K_p(HBO_2)}\sqrt{\frac{k_{s-3}K_p(H_2O)RT}{k_{s-13}}}$
S-19	OBF(g) ---> ^{O}>B-F	$\frac{k_{s-5}k_{s-9}}{k_{s-14}}\frac{K_p(HF)}{K_p(OBF)}\sqrt{\frac{k_{s-13}RT}{k_{s-11}K_p(H_2O)}}$
S-20	B_2O_2(g) ---> ^{O}>B-BO	$\frac{k_{s-6}k_{s-10}k_{s-15}}{k_{s-5}k_{s-6}}\frac{K_p(BF)}{K_p(HF)K_p(B_2O_2)}\sqrt{\frac{k_{s-3}K_p(H_2O)RT}{k_{s-13}}}$

5.0 B2O3(l) GASIFICATION MODEL RESULTS

5.1 Prototypical Example

The species profiles shown in Figure 2 are representative of the gas-phase kinetics associated more with particulate boron combustion than with boron oxide gasification. In particulate boron combustion, boron oxides and fluorides are expected in the reacting mixture. In the present study, the gas-phase kinetics of interest are those between the products of the liquid oxide surface reactions and the species in the surrounding gas-phase environment. In most practical applications of boron as a fuel or propellant additive, the initial composition of the gas-phase environment with which the oxide coated boron particle reacts would be void of boron compounds. Further, the major surface reaction products are expected to be B_2O_3 from vaporization, HBO_2 from the H_2O and HF surface reactions, and OBF from the HF surface reaction.

An example of the homogeneous kinetics in the boundary layer surrounding a gasifying boron oxide droplet is given in Figure 3. Here, the composition of the initial gas-phase equilibrium mixture was derived from a JP-10/air mixture with an oxidizer/fuel ratio of 0.5 in which 10% HF was substituted for 5% O_2 and 5% N_2. To this equilibrium mixture, 3% of the remaining N_2 was replaced by 1% of each of the three surface products: B_2O_3, HBO_2, and OBF. At 1800 K, gas-phase B_2O_3 is converted almost entirely to OBF. In addition, the formation of small amounts of HBO_2 and BF_3 are also predicted. A similar interconversion of boron oxides was reported previously in mixtures without fluorine[1,2] where the equilibrium shift reaction was governed mainly by the overall reaction $B_2O_3 + H_2O = 2HBO_2$. Also, note that the time for formation of OBF and HBO_2 requires a few ms while formation of BF_3 requires approximately one second. Thus, the time to achieve equilibrium in mixtures typical of those surrounding a gasifying droplet can be appreciable.

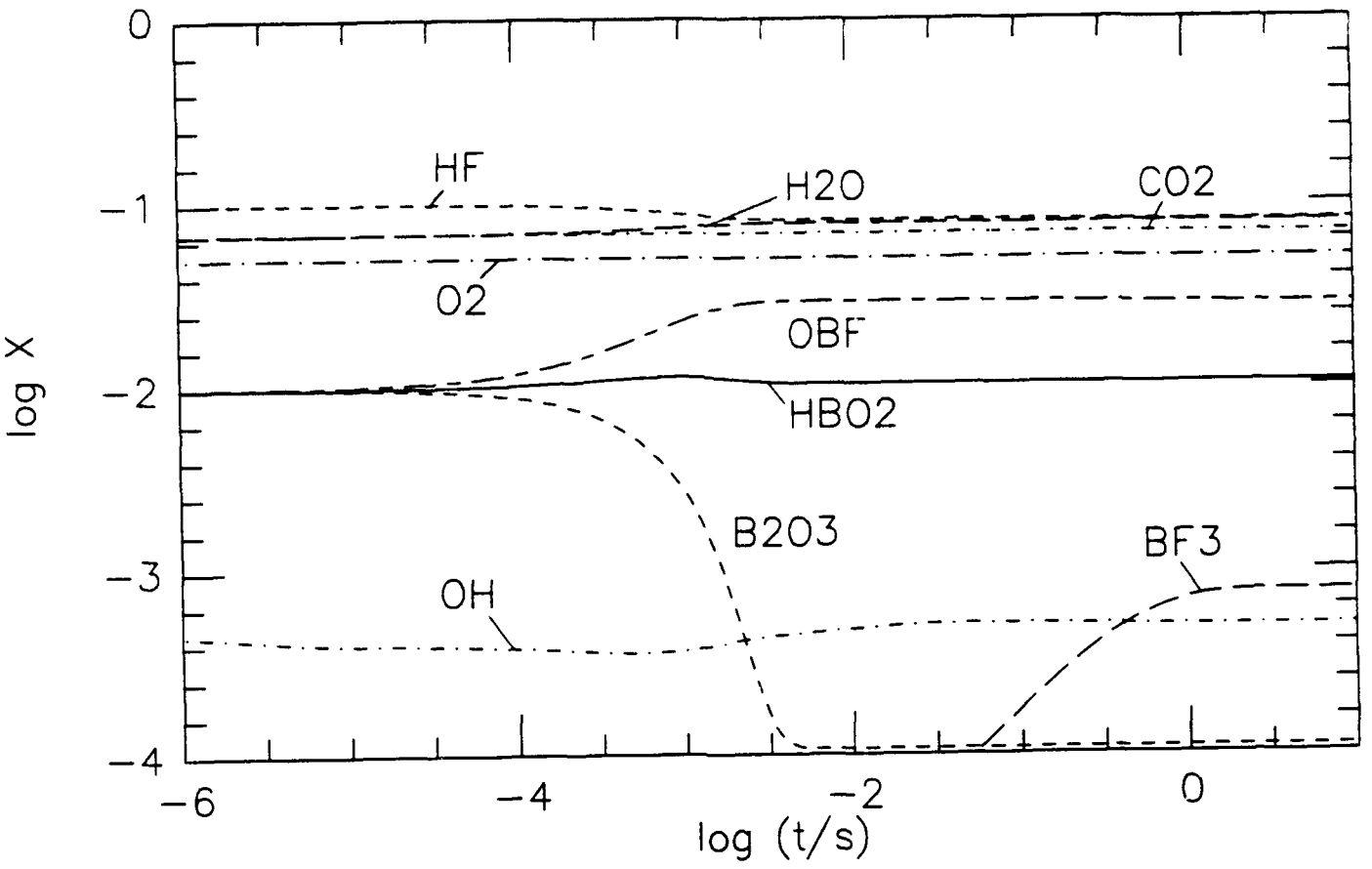

Figure 3. Species profiles for an adiabatic, constant pressure (1 atm) homogeneous system with an initial temperature of 1800 K. The initial mixture consisted of $X(H) = 1.22 \times 10^{-6}$, $X(O) = 3.84 \times 10^{-5}$, $X(OH) = 4.85 \times 10^{-4}$, $X(H_2) = 1.16 \times 10^{-5}$, $X(O_2) = 5.02 \times 10^{-2}$, $X(H_2O) = 6.80 \times 10^{-2}$, $X(HO_2) = 6.40 \times 10^{-7}$, $X(H_2O_2) = 1.92 \times 10^{-8}$, $X(CO) = 4.41 \times 10^{-5}$, $X(CO_2) = 6.82 \times 10^{-2}$, $X(HF) = 1.00 \times 10^{-1}$, $X(N_2) = 6.83 \times 10^{-1}$, $X(B_2O_3) = X(HBO_2) = X(OBF) = 1.00 \times 10^{-2}$.

Species profiles for the quasi-steady gasification of a 500 μm diameter droplet of liquid boron oxide are reported in Figure 4. The ambient temperature is 1800 K and the pressure is 1 atm. The initial gas-phase mixture composition is the same as that reported in Figure 3 without the substitution of the 3% N_2 for the three surface reaction products. In this calculation, the particle diameter is fixed in time, and an equivalent amount of mass is mathematically supplied to the particle as it is consumed. The profiles show that OBF and HBO_2 are the dominant species evolving from the particle surface. BO_2 and B_2O_3 are more than 2 orders of magnitude smaller in concentration than OBF and HBO_2.

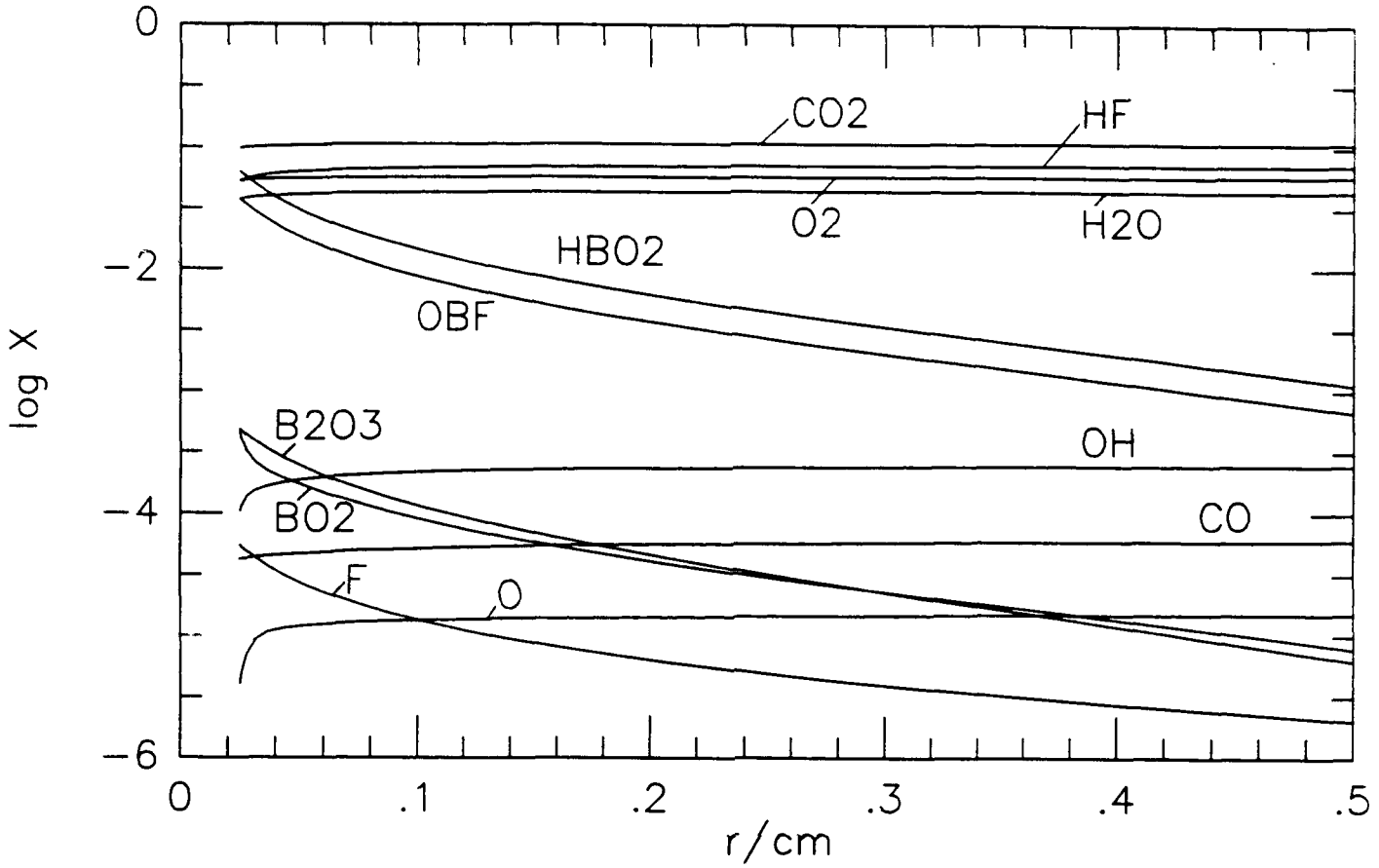

Figure 4. Quasi-steady species mole fraction profiles as a function of normalized position from the surface. The ambient temperature is 1800 K and the particle diameter is 500 μm. The initial mixture consisted of $X(H) = 1.22 \times 10^{-6}$, $X(O) = 3.84 \times 10^{-5}$, $X(OH) = 4.85 \times 10^{-4}$, $X(H_2) = 1.16 \times 10^{-5}$, $X(O_2) = 5.02 \times 10^{-2}$, $X(H_2O) = 6.80 \times 10^{-2}$, $X(HO_2) = 6.40 \times 10^{-7}$, $X(H_2O_2) = 1.92 \times 10^{-8}$, $X(CO) = 4.41 \times 10^{-5}$, $X(CO_2) = 6.82 \times 10^{-2}$, $X(HF) = 1.00 \times 10^{-1}$, $X(N_2) = 7.13 \times 10^{-1}$.

In comparison, the steady-state species profiles for a 500 μm diameter liquid boron oxide droplet in the same gas-phase environment, except with the 10% HF replaced by 5% O_2 and 5% N_2, is given in Figure 5. The results show HBO_2 to be the dominant gas-phase boron-containing species.

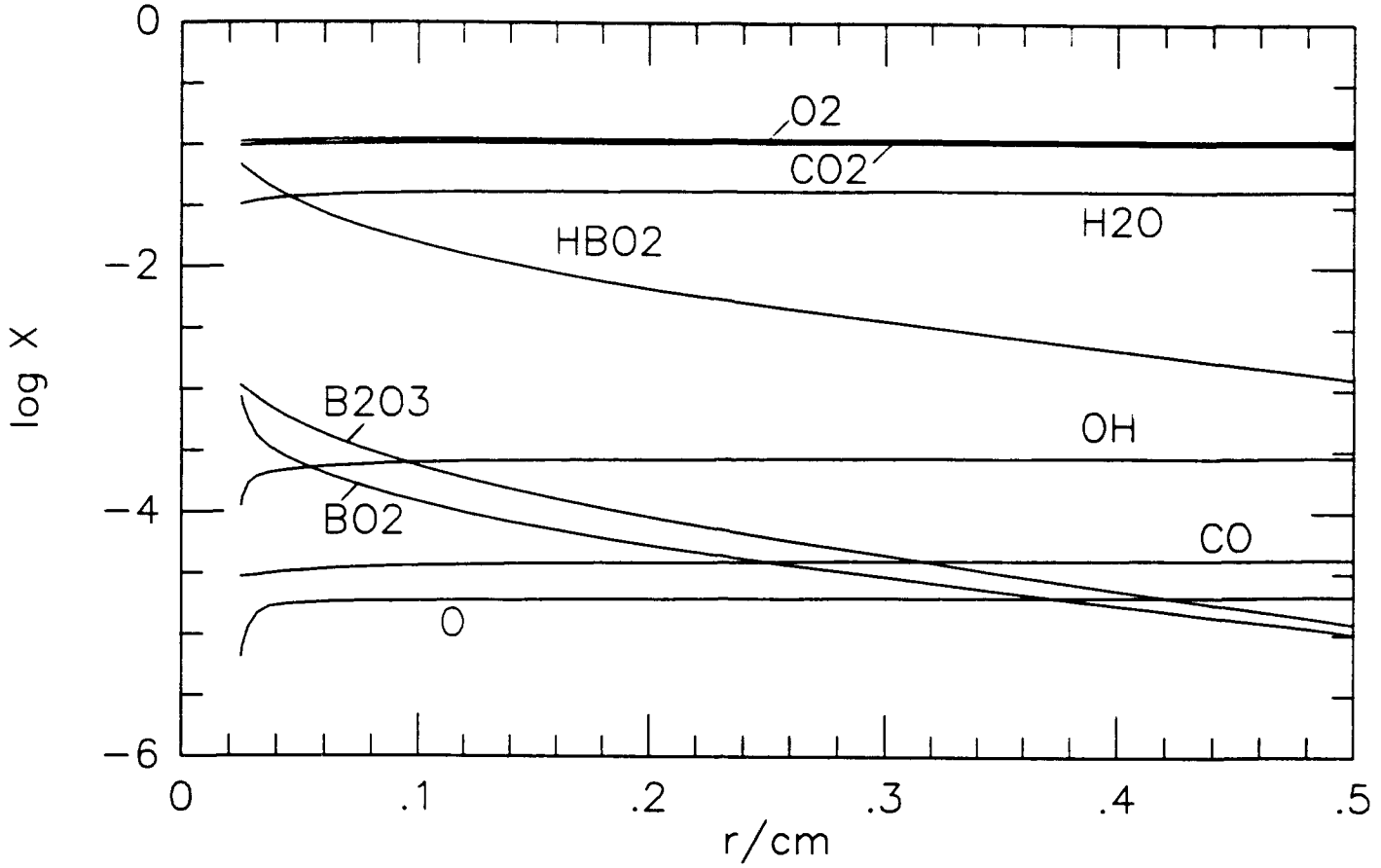

Figure 5. Quasi-steady species mole fraction profiles as a function of normalized position from the surface for a gas-phase environment without fluorine. The ambient temperature is 1800 K and the diameter is 500 μm. The initial mixture consisted of X(H) = 1.22×10^{-6}, X(O) = 3.84×10^{-5}, X(OH) = 4.85×10^{-4}, X(H_2) = 1.16×10^{-5}, X(O_2) = 1.00×10^{-1}, X(H_2O) = 6.80×10^{-2}, X(HO_2) = 6.40×10^{-7}, X(H_2O_2) = 1.92×10^{-8}, X(CO) = 4.41×10^{-5}, X(CO_2) = 6.82×10^{-2}, X(N_2) = 7.63×10^{-1}.

Normalized sensitivity coefficients for the gasification rate with respect to surface kinetic rate constants are reported in Table 13. This table presents the sensitivity gradients, $\ln(K)/\ln(a_j)$ where K is the gasification rate and a_j is a constant parameter of unity value that is associated with each of the surface reaction rate constants. The gasification rate is most sensitive to the adsorption of HF and desorption of ^{O}>B-OH. In contrast, the most sensitive reaction in the system without fluorine is adsorption of H_2O followed by desorption ^{O}>B-OH (see Table 14). However, as shown below, the rate controlling steps of the gasification process are extremely dependent on the size of the droplet, the temperature of the environment, the total amount of reactants in the mixture, and the fluorine to oxygen ratio of the mixture.

Table 13. Most Sensitive Surface Reactions for the System of Figure 4

Reaction	Sensitivity Coefficient
$B_2O_3(l) + HF \rightarrow {}^{O}\!>B\text{-}F + {}^{O}\!>B\text{-}OH$	0.15
${}^{O}\!>B\text{-}OH \rightarrow HBO_2$	0.14
${}^{O}\!>B\text{-}F \rightarrow OBF$	0.06
${}^{O}\!>B\text{-}F + {}^{O}\!>B\text{-}OH \rightarrow B_2O_3(l) + HF$	-0.06
$B_2O_3(l) + H_2O \rightarrow {}^{O}\!>B\text{-}OH + {}^{O}\!>B\text{-}OH$	0.05
${}^{O}\!>B\text{-}OH + {}^{O}\!>B\text{-}OH \rightarrow B_2O_3(l) + H_2O$	-0.04

Table 14. Most Sensitive Surface Reactions for the System of Figure 5

Reaction	Sensitivity Coefficient
$B_2O_3(l) + H_2O \rightarrow {}^{O}\!>B\text{-}OH + {}^{O}\!>B\text{-}OH$	0.27
${}^{O}\!>B\text{-}OH \rightarrow HBO$	20.19
${}^{O}\!>B\text{-}OH + {}^{O}\!>B\text{-}OH \rightarrow B_2O_3(l) + H_2O$	-0.09
$B_2O_3(l) + OH \rightarrow {}^{O}\!>B\text{-}O + {}^{O}\!>B\text{-}OH$	0.02

The time dependent rate of gasification, in units of surface area per second, for the system in Figure 4 is shown in Figure 6. In this calculation, the particle radius was not fixed in time, but allowed to regress as the oxide was gasified from the surface. At 21 sec, the diameter of the droplet is approximately 100 μm. In comparison, the time dependent gasification rate for the system without fluorine is also shown in Figure 6. The results show the gasification rate to increase with addition of HF. Without fluorine, the diameter of the droplet equals 100 μm at approximately 33 sec. Note that during the first 80% change in diameter, the gasification rate drops by 30-40%, before decreasing significantly more during the final stages of gasification.

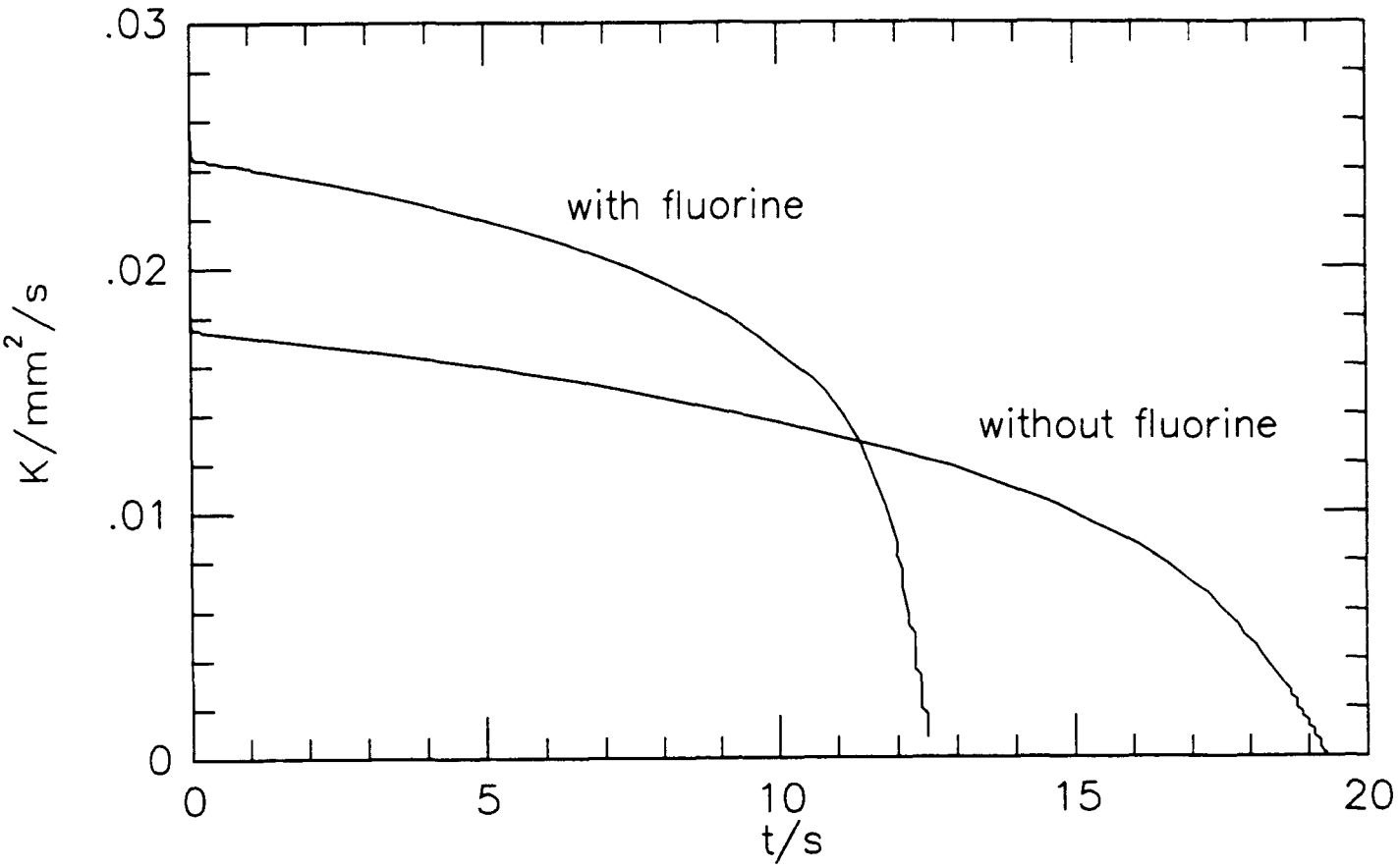

Figure 6. Gasification rate as a function of time for gas compositions with fluorine (Figure 3) and without fluorine (Figure 4) with an initial temperature of 1800 K and an initial particle diameter of 500 μm.

5.2 Effect of Droplet Diameter

The effect of the droplet diameter on the gasification rate is given in Figure 7. The range of diameters studied was 2000 μm to 20 μm. The gas-composition, temperature, and pressure of the surrounding environment was the same as that of Figure 4. Gasification rates for both fixed diameter droplets and for three regressing diameter droplets are presented. The symbols indicate the gasification rates for each of the fixed diameter calculations. The solid lines show the time dependent trajectories of droplets with initial diameters of 2000, 1000, and 500 μm. fixed diameter results show the gasification rate to increase rapidly for particle diameters up to approximately 500 μm and to be nearly independent of the diameter for droplets with diameters greater than 1000 μm. Classical theory predicts the gasification rate to be independent of diameter if the process is diffusion controlled and to be linearly dependent on the diameter if the rate is kinetically controlled. The present results predict both regimes at the smallest and largest diameters studied. However, the transition from the kinetically controlled to diffusion controlled rate occurs over an extremely wide range of diameters.

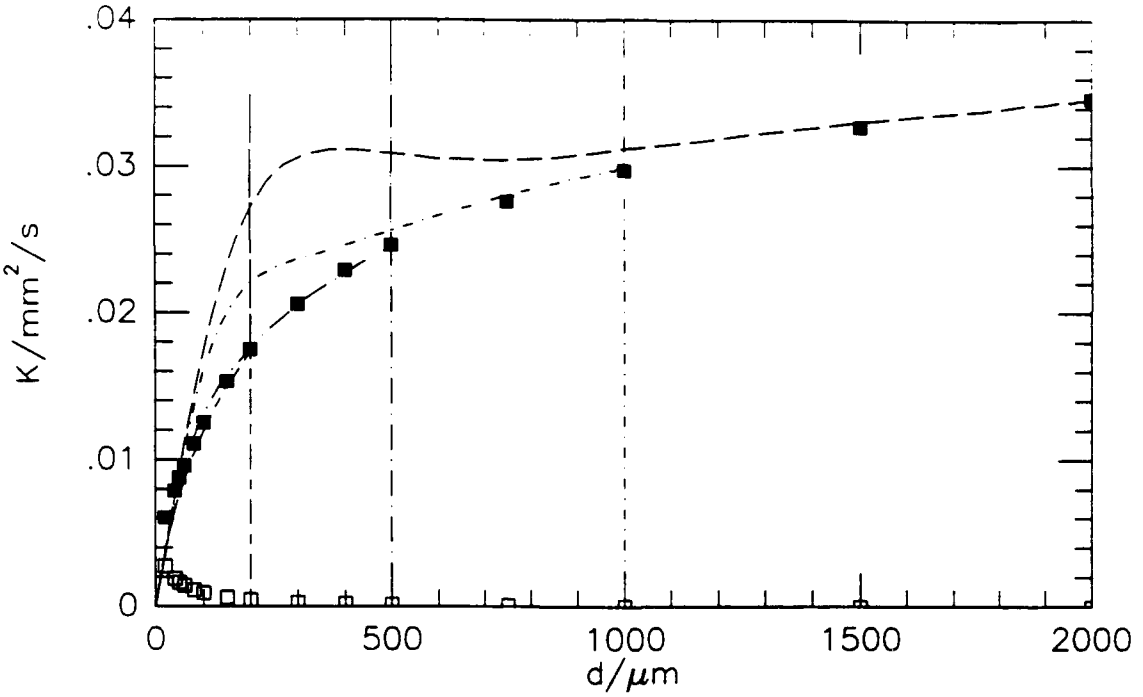

Figure 7. Gasification rates of liquid B_2O_3 droplets as a function of diameter. The initial surrounding gas-phase environment consisted of $X(H) = 1.22\times10^{-6}$, $X(O) = 3.84\times10^{-5}$, $X(OH) = 4.85\times10^{-4}$, $X(H_2) = 1.16\times10^{-5}$, $X(O_2) = 5.02\times10^{-2}$, $X(H_2O) = 6.80\times10^{-2}$, $X(HO_2) = 6.40\times10^{-7}$, $X(H_2O_2) = 1.92\times10^{-8}$, $X(CO) = 4.41\times10^{-5}$, $X(CO_2) = 6.82\times10^{-2}$, $X(HF) = 1.00\times10^{-1}$, and $X(N_2) = 7.13\times10^{-1}$ with an initial temperature of 1800 K and pressure of one atmosphere. The squares are the steady-state gasification rates obtained when the diameter is not allowed to regress. The solid lines are the transient gasification rates as a function of diameter as the droplet is consumed. Data for the transient calculations are presented for initial diameters of 2000, 1000, 500, and 200 μm.

The regressing surface results also reveal that for initial droplet diameters less than about 500 μm, the time dependent gasification rate closely follows the fixed diameter gasification rates as the diameter is decreased. However, for droplets with initial diameters greater than 500 μm, the rates are predicted to deviate substantially from the fixed diameter predictions. This deviation is due to the build-up of surface products in a boundary layer surrounding the particle, thus significantly altering the reactants attacking the surface.

Surface reaction rates for the fixed diameter calculations as a function of diameter are presented in Figure 8. Desorption of the $^{O}>$B-OH surface complex is the fastest step at small diameters while adsorption of HF is the fastest step for large diameter droplets. For small diameter droplets, the surface reactions are far from equilibrium whereas for large diameters, the surface reactions are nearly equilibrated.

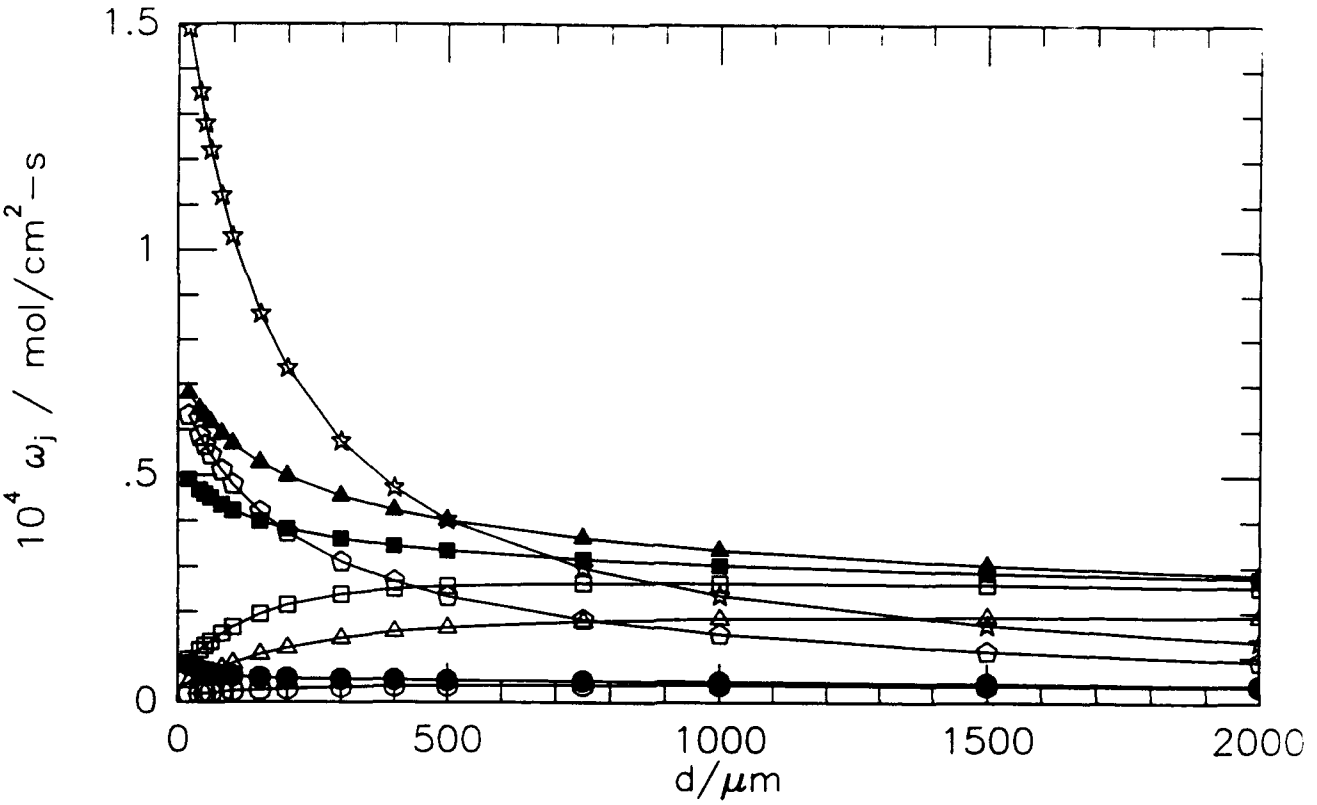

Figure 8. Surface reaction flux profiles for the steady-state results presented in Figure 7. The symbols denote the surface reactions as follows: S-1, solid diamond; S-2, solid circle; S-3, solid square; S-4, inverted solid triangle; S-5, solid triangle; S-7, four pointed star; S-8 five pointed star; S-9, open pentagon; S-11, open diamond; S-12, open circle; S-13, open square; S-14, inverted open triangle; S-15, open triangle; S-17, four pointed cross "x"; S-18, five pointed cross; S-19, solid pentagon. See Tables 7-10 for definitions of the surface reaction numbers.

The most sensitive surface reactions, as a function of droplet diameter, are reported in Figure 9. Adsorption of HF is the most sensitive reaction for all diameters except 20 μm. At 20 μm, adsorption of H_2O is most sensitive, but decreases in importance as the diameter is increased. Interestingly, the effect that H_2O adsorption has on the gasification rate changes at a diameter of about 150 μm (as indicated by a change in sign of the gradient). For diameters less than 150 μm, this reaction tends to increase the gasification rate, whereas for diameters greater than 150 μm, it tends to decrease the gasification rate. Desorption of $^{O}>$B-OH follows a similar trend, enhancing gasification for diameters smaller than 400 μm and inhibiting gasification for diameters greater than 400 μm. In contrast, the gasification rate becomes increasingly more sensitive to the desorption of the $^{O}>$B-F complex as the diameter is increased.

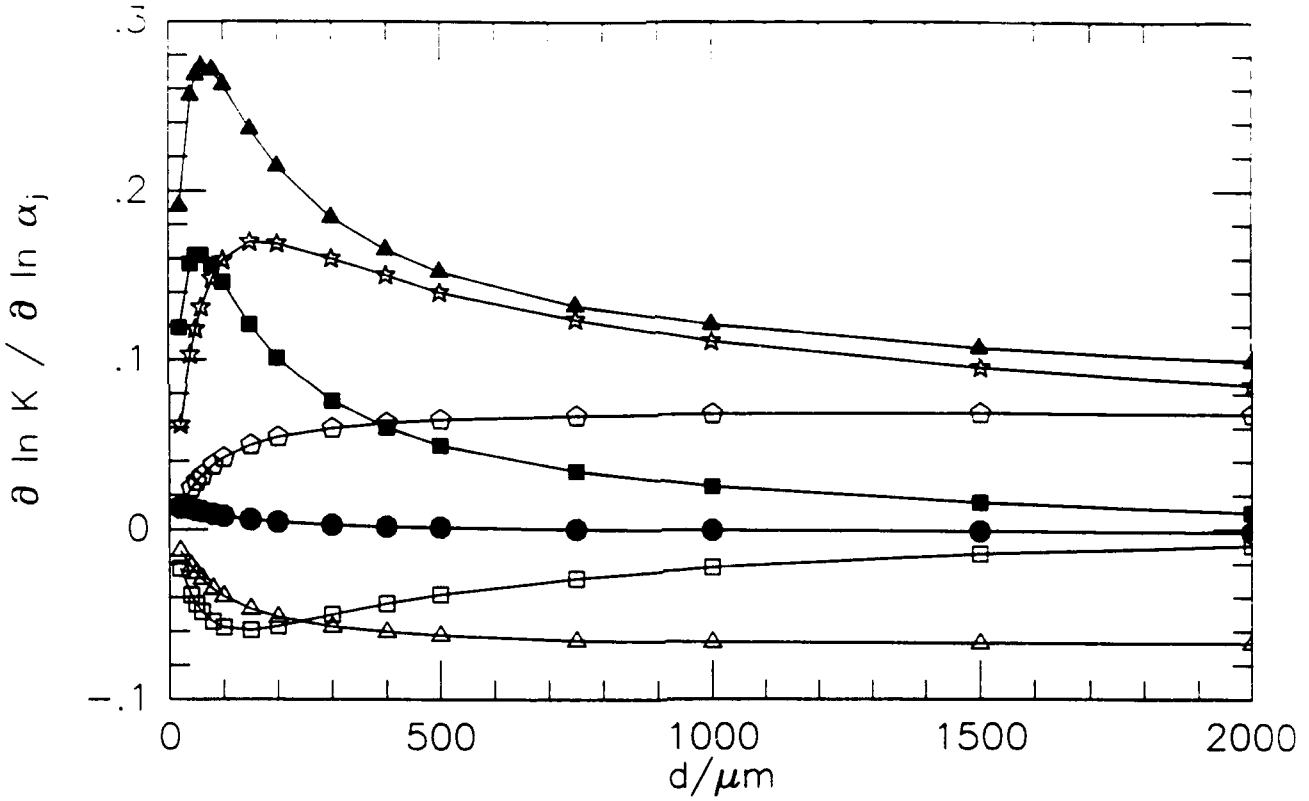

Figure 9. Sensitivity gradient profiles, $\ln K/\ln(a_j)$, of the response of the gasification rate to variations in the rate parameters of the surface reactions. K is the gasification rate and aj is a constant parameter of unity value that is associated with each of the surface reaction rate constants. The calculations are for the steady-state results presented in Figure 7. The symbols denote the surface reactions as follows: S-1, solid diamond; S-2, solid circle; S-3, solid square; S-4, inverted solid triangle; S-5, solid triangle; S-7, four pointed star; S-8 five pointed star; S-9, open pentagon; S-11, open diamond; S-12, open circle; S-13, open square; S-14, inverted open triangle; S-15, open triangle; S-17, four pointed cross "x"; S-18, five pointed cross; S-19, solid pentagon. See Tables 7-10 for definitions of the surface reaction numbers.

5.3 Effect of Gas Phase Temperature

An increase in the environmental temperature results in a change in the composition of the gas surrounding the droplet. Given the same elemental composition as studied in the previous examples, the change in equilibrium mixture composition with temperature is shown in Figure 10. The major stable species HF, H_2O, CO_2, and O_2 remain nearly constant while the transient radicals, OH, O, and H, and the dissociation products CO and H_2 increase by 1-2 orders of magnitude in concentration over the temperature range of 1600 to 2050 K. Thus, a change in temperature can alter the gasification rate by changing the rate constants and by changing the speciation of reactants.

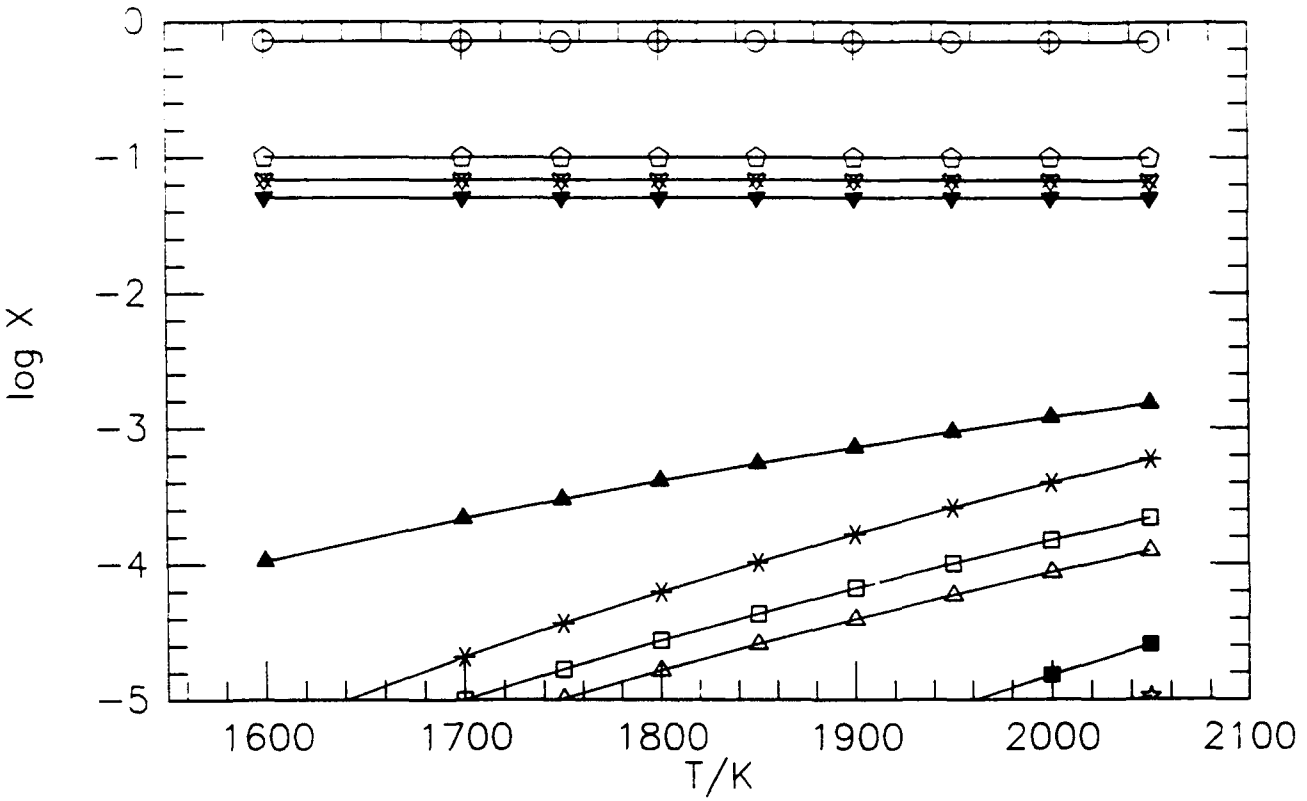

Figure 10. Equilibrium mixture composition as a function of temperature. The mixture is based on the environmental composition of Figure 6.

The effect of temperature on the steady-state gasification rate is shown in Figure 11 for a 50 μm diameter droplet. The calculations were performed with a fixed diameter droplet. The gasification rate is predicted to increase with temperature. The increase in rate results from the increased rate of surface reactions, the increased rate of vaporization, and the increase in radical concentrations in the surrounding gas. Below 1950 K, the gasification process is dominated by surface reactions. Between 1950 and 2050 K, vaporization plays a equally important role in gasifying the liquid boron oxide droplet.

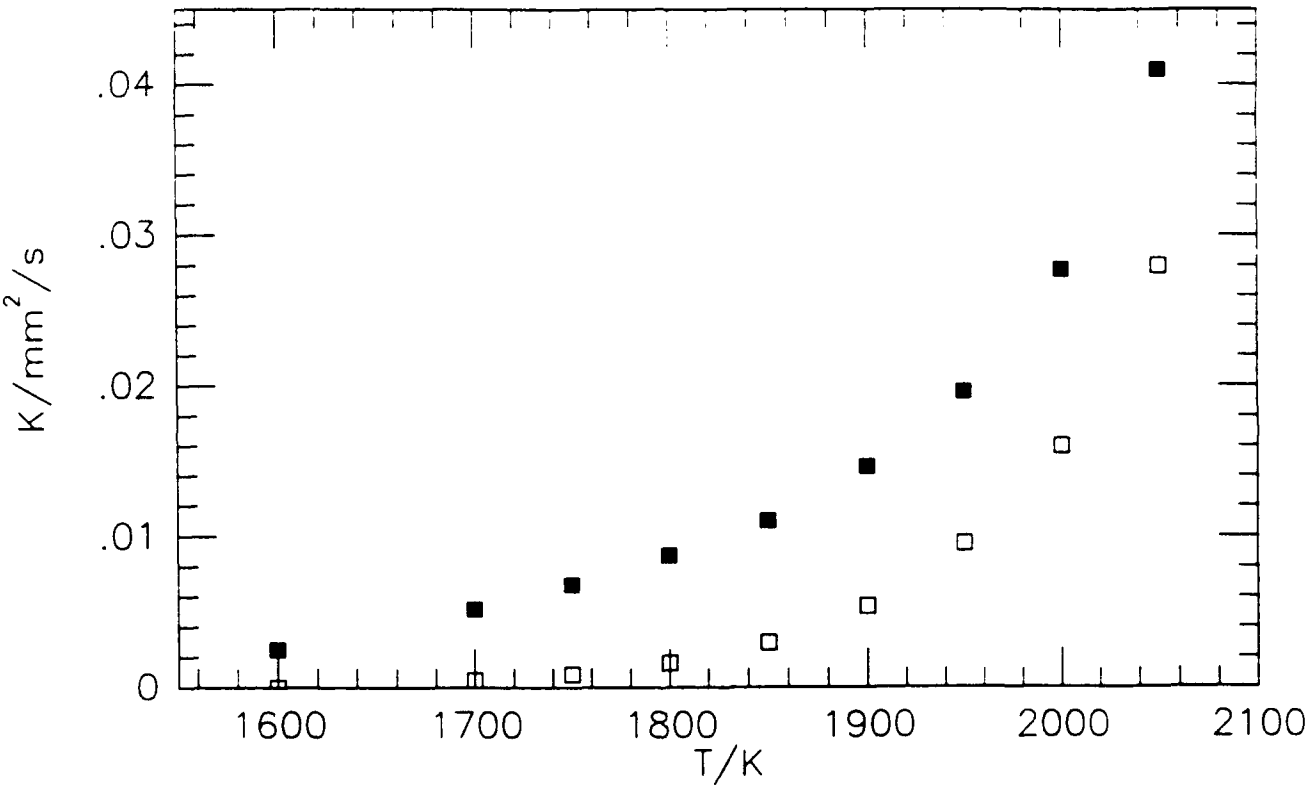

Figure 11. Gasification rates of liquid B_2O_3 as a function of temperature. The initial mixture compositions are presented in Figure 10. All the calculations are for a fixed particle diameter of 50 μm.

The rates of the individual surface reactions as a function of temperature are presented in Figure 12. The desorption of the ^{O}>B-OH complex to form $HBO_2(g)$ increases the most rapid with temperature followed by the desorption of the ^{O}>B-F complex to form OBF(g). Reaction of the oxide layer with HF and H_2O are the fastest adsorption reactions. How-ever, surface reaction by OH becomes appreciable above 1800 K. The rates of the second order desorption reactions are predicted to decrease with temperature.

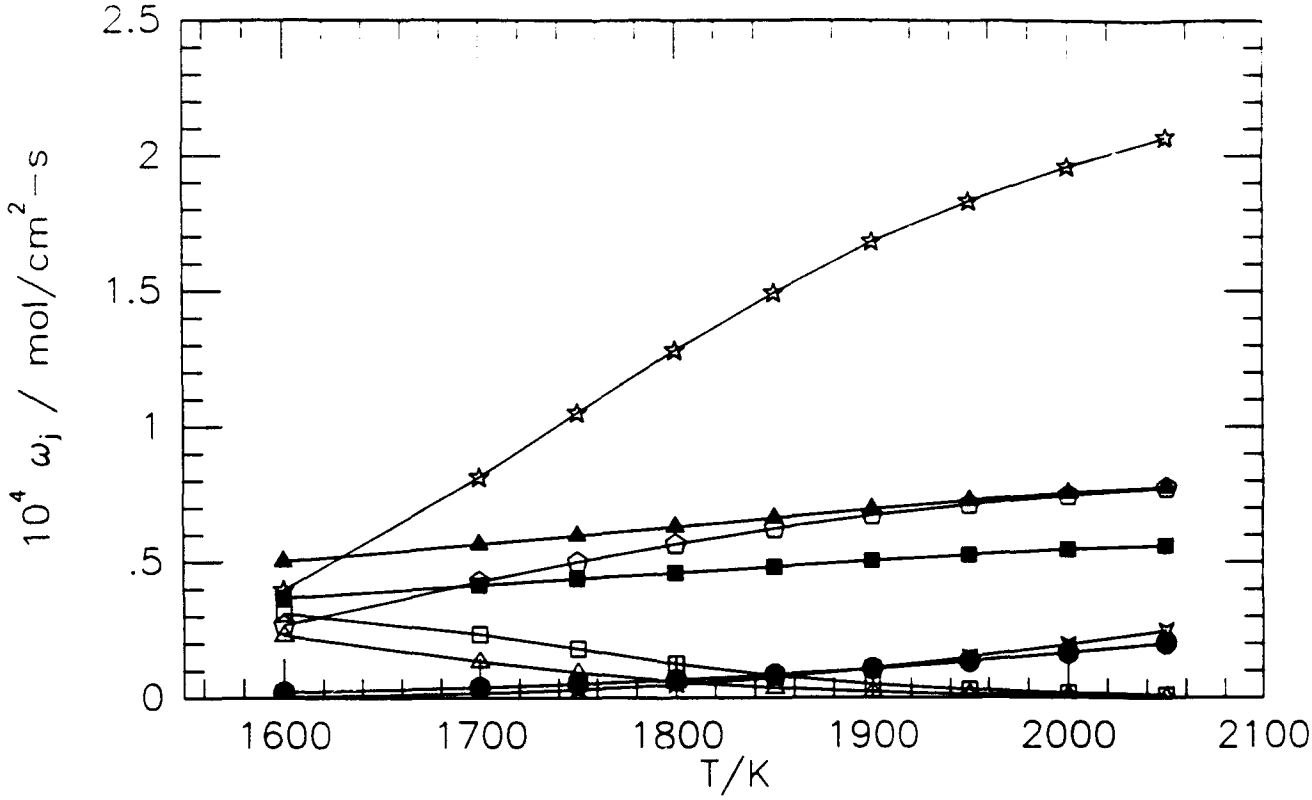

Figure 12. Surface reaction flux profiles for the steady-state results presented in Figure 11. The symbols denote the surface reactions as follows: S-1, solid diamond; S-2, solid circle; S-3, solid square; S-4, inverted solid triangle; S-5, solid triangle; S-7, four pointed star; S-8 five pointed star; S-9, open pentagon; S-11, open diamond; S-12, open circle; S-13, open square; S-14, inverted open triangle; S-15, open triangle; S-17, four pointed cross "x"; S-18, five pointed cross; S-19, solid pentagon. See Tables 7-10 for definitions of the surface reaction numbers

The most sensitive surface reactions on the gasification process are given in Figure 13. The rapid increase in sensitivity of desorption reactions with decreasing temperature is indicative of their rate limiting role below 1600 K for the droplet and mixture composition under consideration here. Above 1700 K, the rate limiting processes are shown to be adsorption reactions. However, note that between 1950 and 2000 K, an increase in the rate of the three adsorption processes of HF, H_2O, and OH changes from one of acceleration to one of inhibition. This change in behavior is accompanied by a simultaneous increase in the vaporization process.

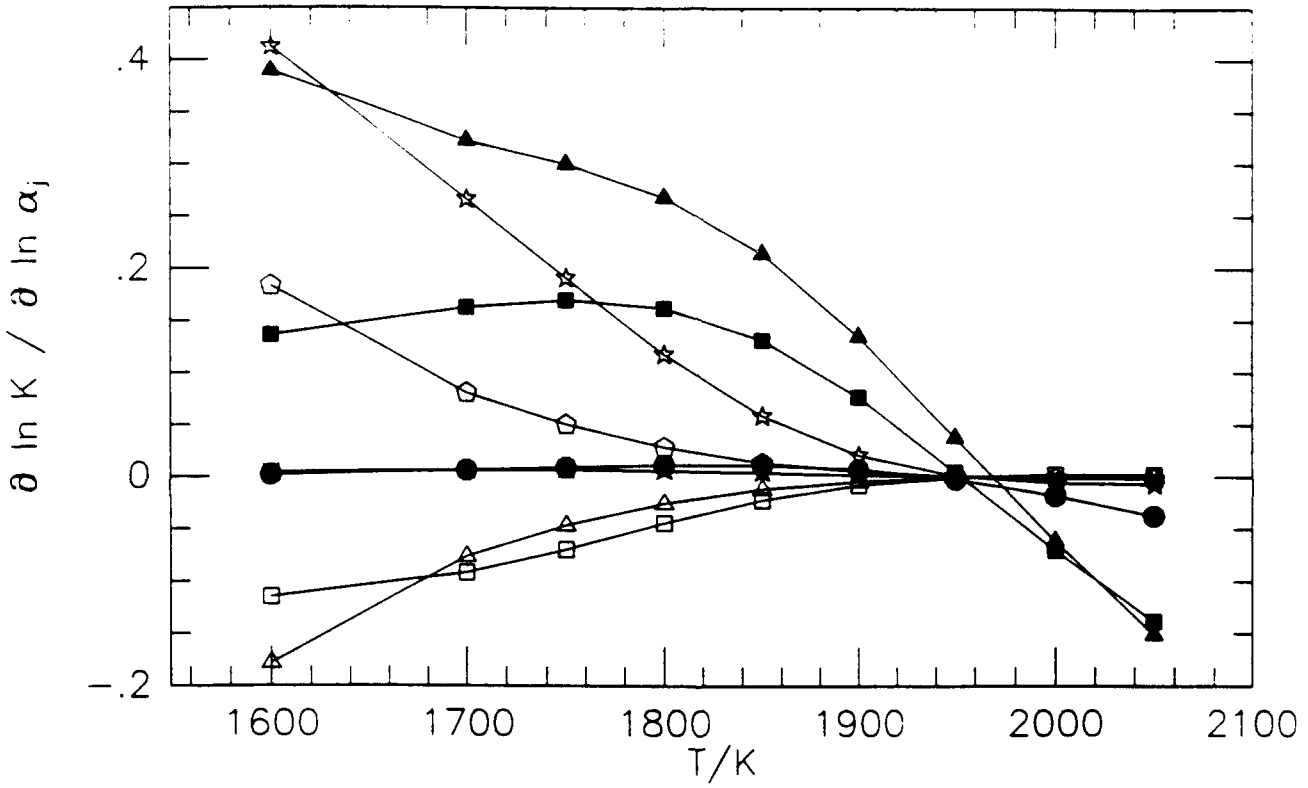

Figure 13. Sensitivity gradient profiles of the response of the gasification rate to variations in the rate parameters of the surface reactions. The calculations are for the steady-state results presented in Figure 11. The symbols denote the surface reactions as follows: S-1, solid diamond; S-2, solid circle; S-3, solid square; S-4, inverted solid triangle; S-5, solid triangle; S-7, four pointed star; S-8 five pointed star; S-9, open pentagon; S-11, open diamond; S-12, open circle; S-13, open square; S-14, inverted open triangle; S-15, open triangle; S-17, four pointed cross "x"; S-18, five pointed cross; S-19, solid pentagon. See Tables 7-10 for definitions of the surface reaction numbers

5.4 Effect of Dilution

With N_2 as the only nitrogen-containing species in the gas-phase mechanism, the effect of varying the N_2 content in the surrounding equilibrium mixture is simply dilution as shown in Figure 14. A decrease in the N_2 content of the mixture results in an increase in the partial pressures of each of the reactants, which produces an increase in the gasification rate as shown in Figure 15. Compared to the pure vaporization rate (100% N_2), the gasification rate is increased by about a factor of 5 when the N_2 is totally replaced by the H/O/C/F mixture. As the nitrogen content of the mixture is decreased from 100%, the rates of the first-order surface reactions are predicted to increase the fastest (see Figure 16). However, by 30% reduction in the N_2 content, the rates of increase of the second-order surface reactions exceed those of first-order surface reactions. Sensitivity gradient profiles (Figure 17) show the adsorption of HF to be the most sensitive reaction followed by the desorption of the surface complex $O_{>}B\text{-}OH$ or the adsorption of H_2O, depending on the N_2 content. The rate limiting nature of the adsorption reactions is predicted to decrease relative to the desorption reactions with an decrease in N_2 content.

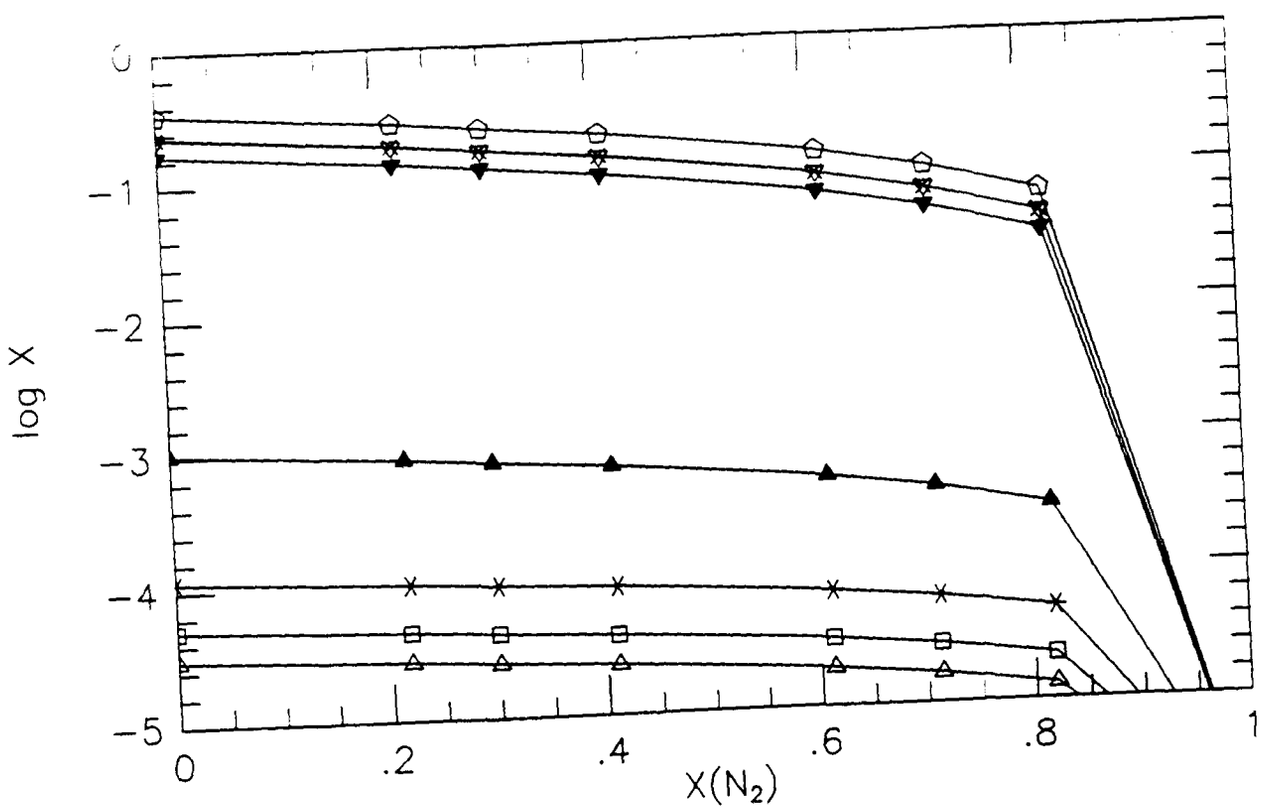

Figure 14. Equilibrium mixture composition as a function of N_2 content. The mixture is based on the environmental composition of Figure 6.

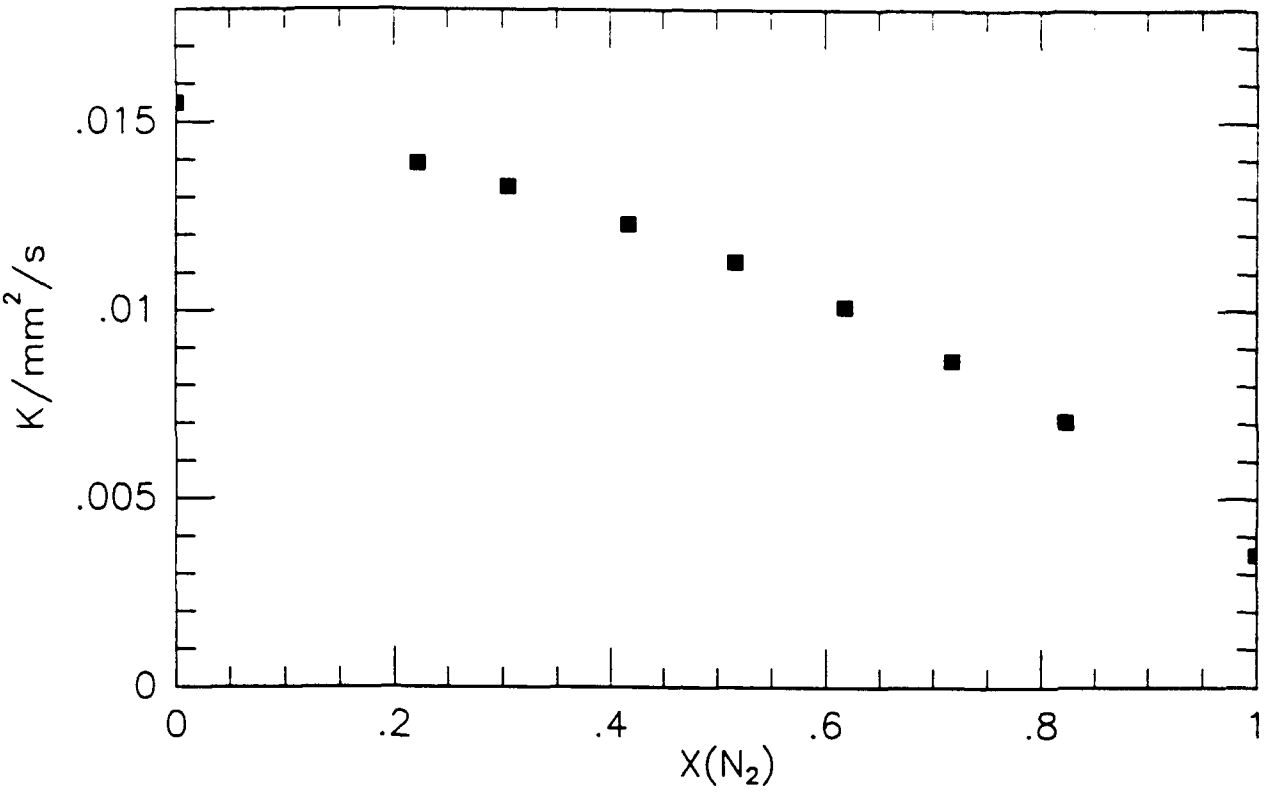

Figure 15. Gasification rates of liquid B_2O_3 as a function of N_2 content in the mixture. The initial mixture compositions are presented in Figure 14. All the calculations are for a fixed diameter droplet of 50 μm.

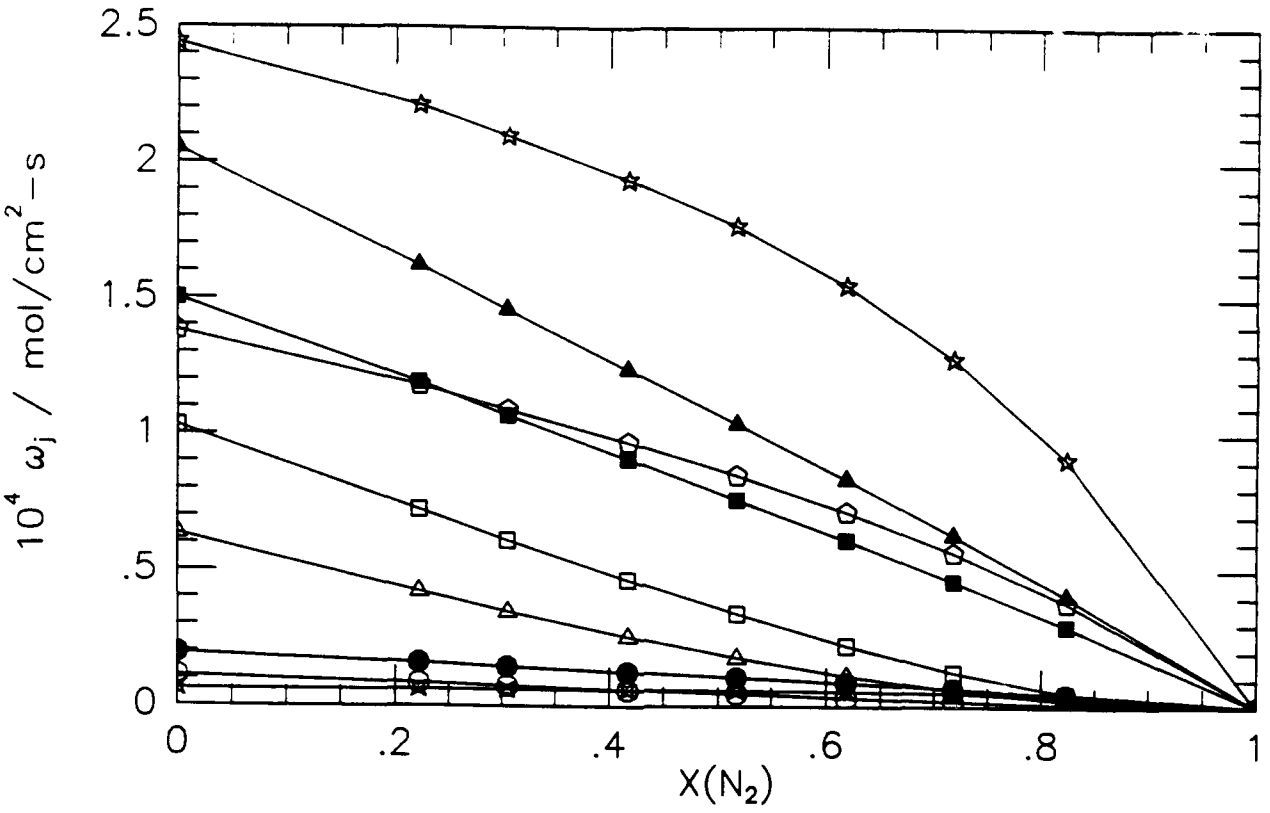

Figure 16. Surface reaction flux profiles for the steady-state results presented in Figure 15. The symbols denote the surface reactions as follows: S-1, solid diamond; S-2, solid circle; S-3, solid square; S-4, inverted solid triangle; S-5, solid triangle; S-7, four pointed star; S-8 five pointed star; S-9, open pentagon; S-11, open diamond; S-12, open circle; S-13, open square; S-14, inverted open triangle; S-15, open triangle; S-17, four pointed cross "x"; S-18, five pointed cross; S-19, solid pentagon. See Tables 7-10 for definitions of the surface reaction numbers

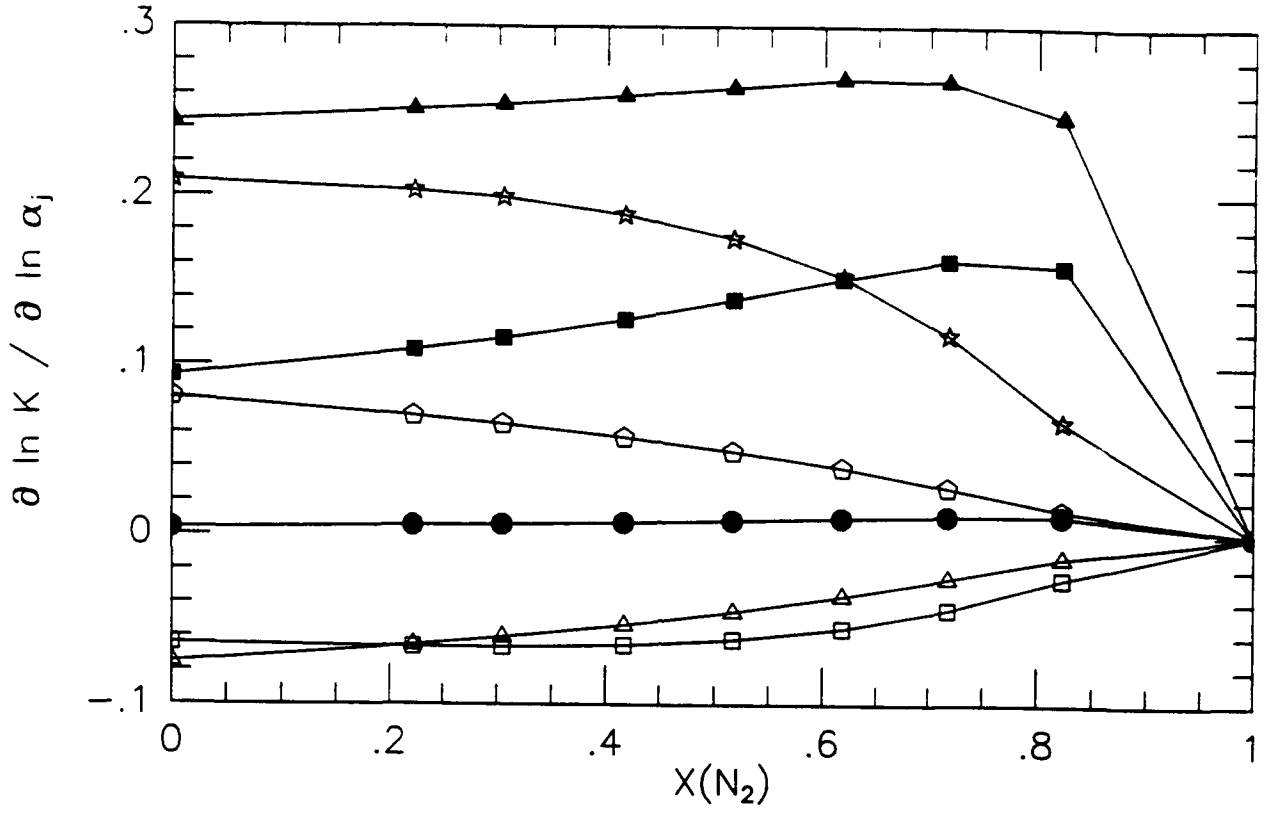

Figure 17. Sensitivity gradient profiles of the response of the gasification rate to variations in the rate parameters of the surface reactions. The calculations are for the steady-state results presented in Figure 15. The symbols denote the surface reactions as follows: S-1, solid diamond; S-2, solid circle; S-3, solid square; S-4, inverted solid triangle; S-5, solid triangle; S-7, four pointed star; S-8 five pointed star; S-9, open pentagon; S-11, open diamond; S-12, open circle; S-13, open square; S-14, inverted open triangle; S-15, open triangle; S-17, four pointed cross "x"; S-18, five pointed cross; S-19, solid pentagon. See Tables 7-10 for definitions of the surface reaction numbers.

5.5 Effect of Fluorine/Oxygen Mole Ratio

The fluorine/oxygen (F/O) ratio in the gas-phase environment can be varied in several manners. In the first two examples presented here, the F/O ratio was varied without holding the hydrogen content fixed. In Figure 18, the F/O ratio of the gas-phase equilibrium mixture was varied by fixing separately the nitrogen, carbon, and hydrogen atom balances and the sum of the oxygen and fluorine atom balance. The mixture composition shows the CO_2 mole fraction to remain nearly the same as the F/O ratio is increased until a ratio of about 1.6, at which point the CO mole fraction increases rapidly. The H_2O and OH mole fractions decrease with increasing F/O and are essentially eliminated from the mixture at an F/O ratio near 1.4. At the same F/O ratio, a significant increase in the F-atom mole fraction is observed. The HF mole fraction increases and the O_2 mole fraction decreases with increasing F/O ratio.

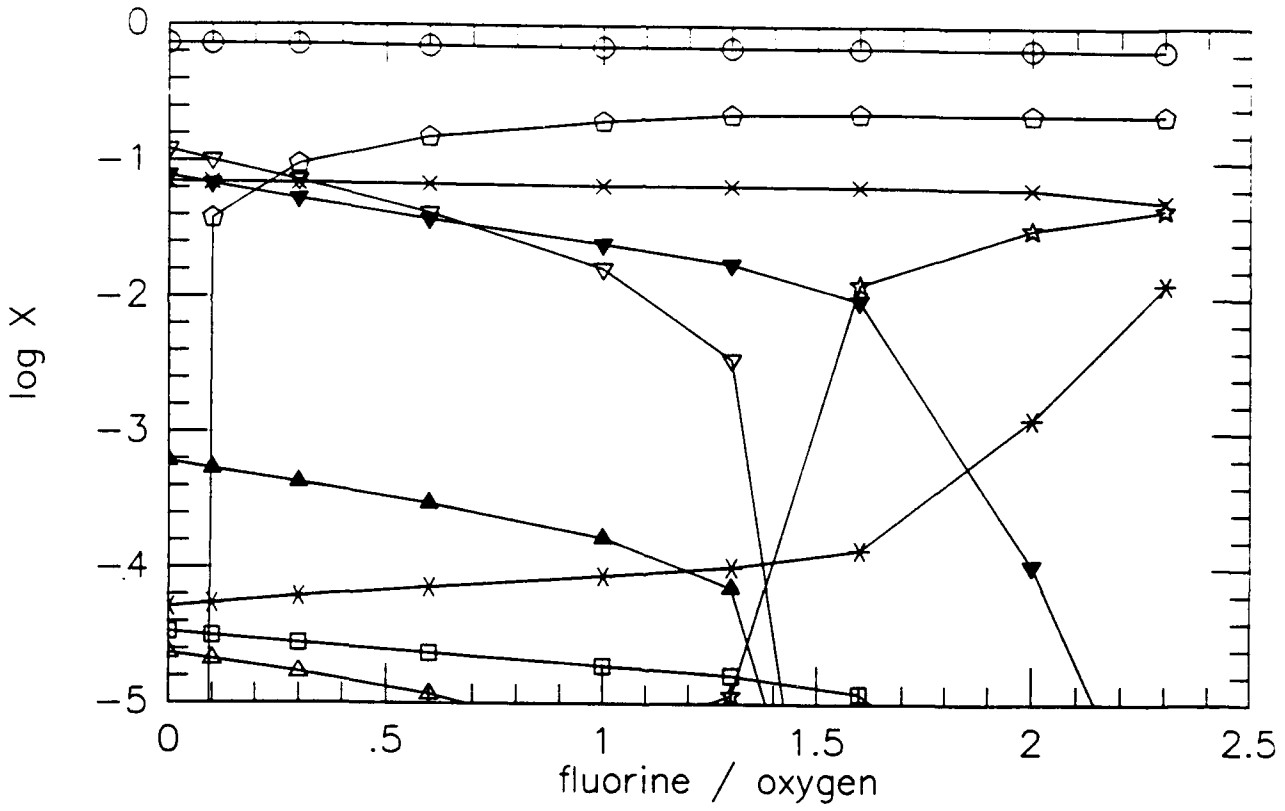

Figure 18. Equilibrium mixture composition as a function of fluorine/oxygen mole ratio. The mixture is based on the environmental composition of Figure 6.

The gasification rates of a 50 μm diameter droplet with the mixture compositions shown in Figure 17 and an ambient temperature of 1800 K and pressure of 1 atm are shown in Figure 19. The results show that addition of a small amount of fluorine to the mixture (F/O = 0.1) increases the gasification rate by approximately 16%. Further increasing the F/O ratio to 1.3 increases the gasification rate by 23%. Interestingly, an increase in the F/O from 1.3 to 2.3 increases the gasification rate by 78%. The sudden increase in the gasification rate at a F/O ratio of 1.3 corresponds to the mixture where the H_2O and OH concentrations are eliminated from the mixture and the F-atom concentration is significantly increased.

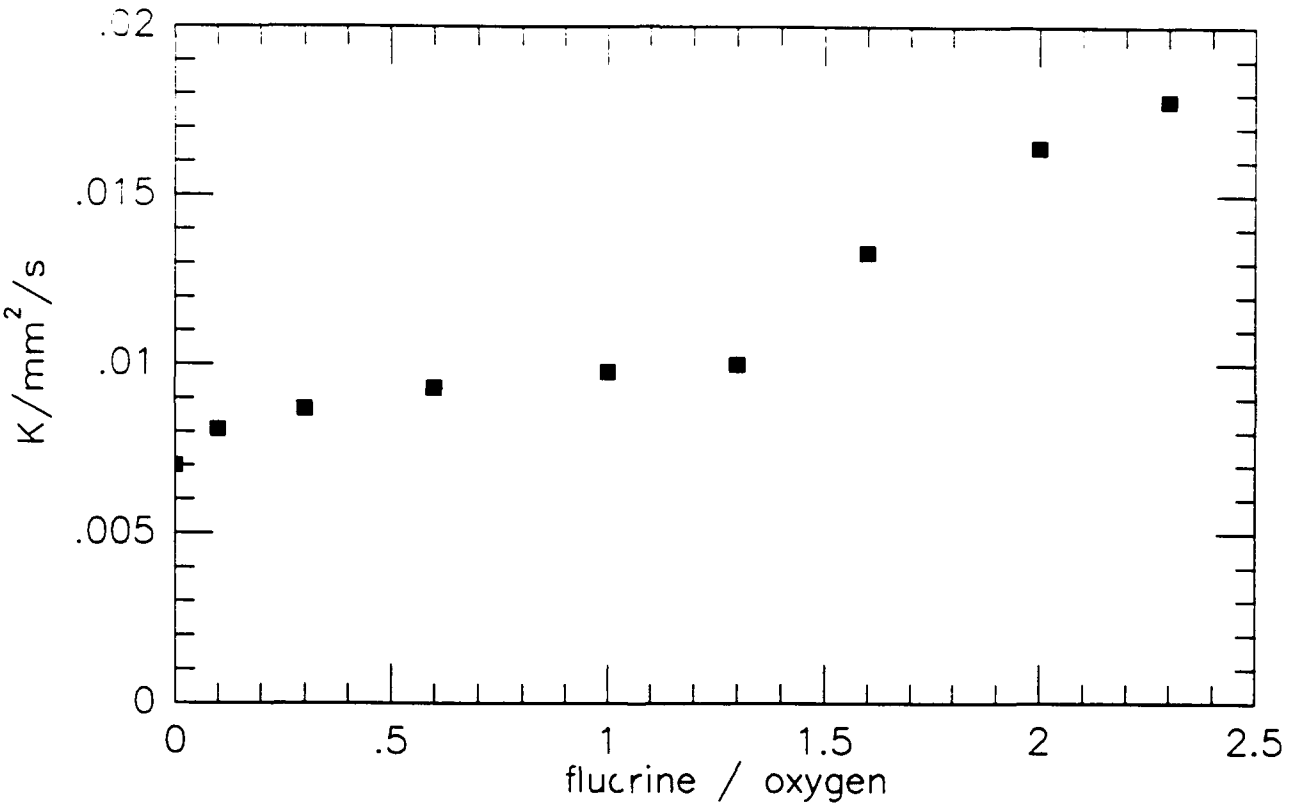

Figure 19. Gasification rates of liquid B_2O_3 as a function of the F/O ratio in the surrounding mixture. The initial mixture compositions are presented in Figure 18. All the calculations are for a fixed diameter droplet of 50 μm.

The fastest and the rate limiting surface reactions as a function of F/O ratio are given in Figures 20 and 21, respectively. The reaction flux results show a significant increase in the rate of F-atom adsorption on the surface at a F/O ratio of 1.3. The sensitivity gradient results show H_2O adsorption to be most sensitive for F/O < 0.25, HF adsorption to be most sensitive for 0.25 < F/O < 1.8, and F-atom adsorption to be most sensitive for F/O > 1.8.

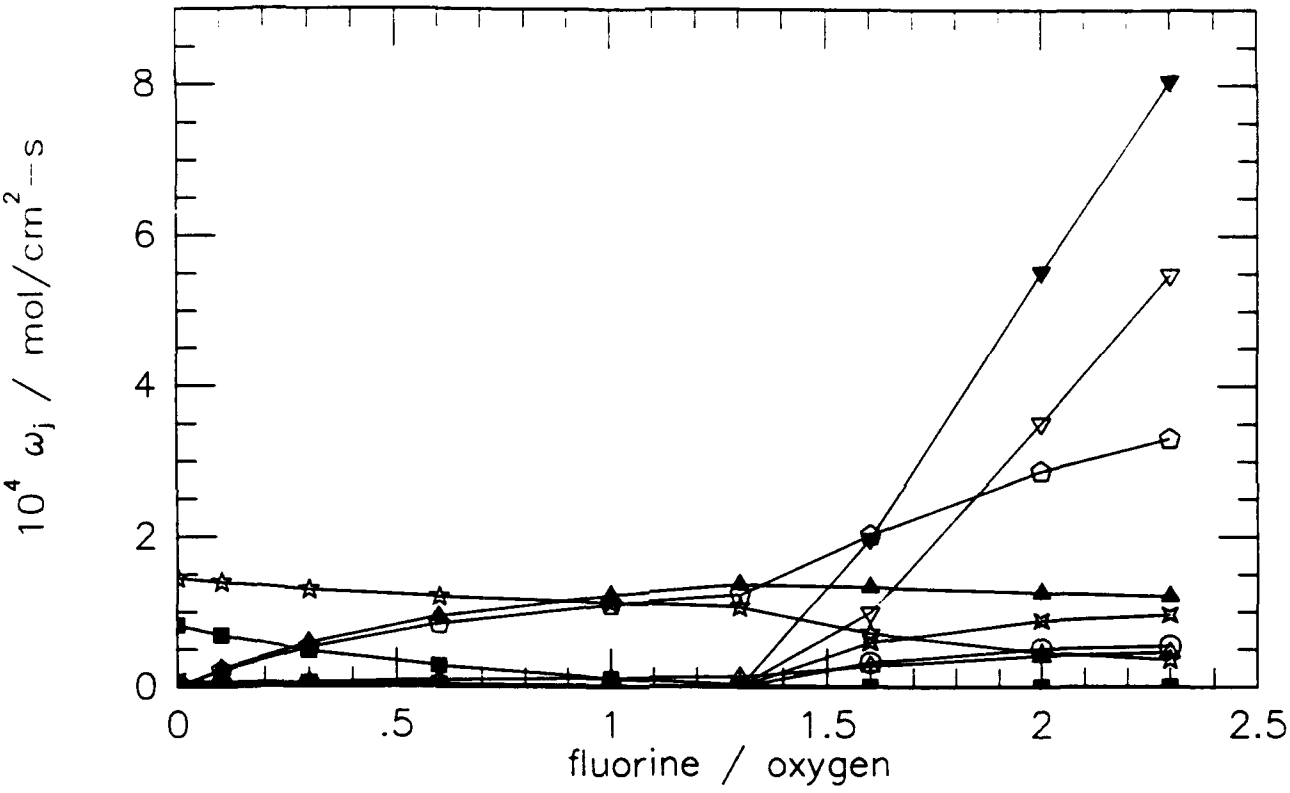

Figure 20. Surface reaction flux profiles for the steady-state results presented in Figure 18. The symbols denote the surface reactions as follows: S-1, solid diamond; S-2, solid circle; S-3, solid square; S-4, inverted solid triangle; S-5, solid triangle; S-7, four pointed star; S-8 five pointed star; S-9, open pentagon; S-11, open diamond; S-12, open circle; S-13, open square; S-14, inverted open triangle; S-15, open triangle; S-17, four pointed cross "x"; S-18, five pointed cross; S-19, solid pentagon. See Tables 7-10 for definitions of the surface reaction numbers.

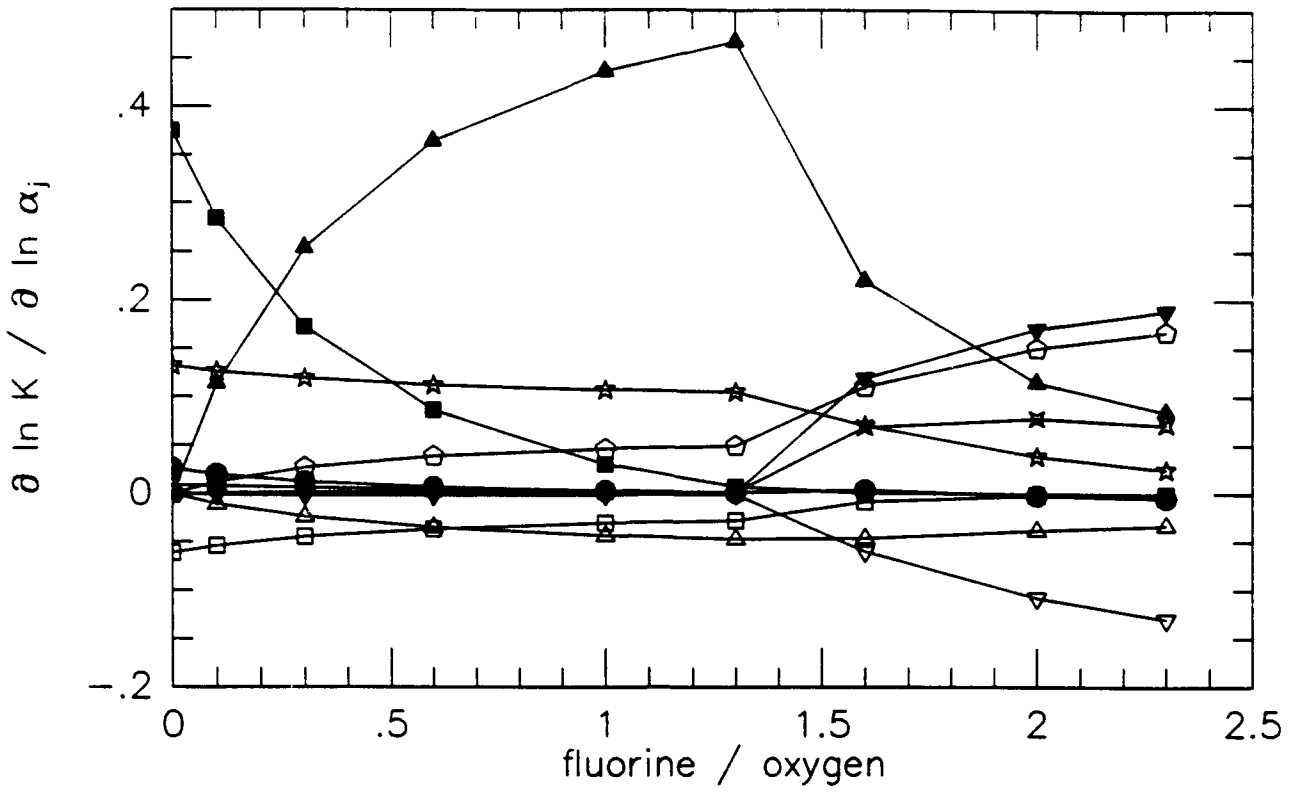

Figure 21. Sensitivity gradient profiles of the response of the gasification rate to variations in the rate parameters of the surface reactions. The calculations are for the steady-state results presented in Figure 18.The symbols denote the surface reactions as follows: S-1, solid diamond; S-2, solid circle; S-3, solid square; S-4, inverted solid triangle; S-5, solid triangle; S-7, four pointed star; S-8 five pointed star; S-9, open pentagon; S-11, open diamond; S-12, open circle; S-13, open square; S-14, inverted open triangle; S-15, open triangle; S-17, four pointed cross "x"; S-18, five pointed cross; S-19, solid pentagon. See Tables 7-10 for definitions of the surface reaction numbers.

6.0 SUMMARY AND CONCLUSIONS

In summary, a model has been developed to describe the gasification of a liquid boron oxide droplet in combustion environments having a gas phase speciation similar to that expected in the post-combustion environment of advanced fluoroamino/nitroamino based oxidizers. The model includes the gas phase B/H/O/C/F kinetics formulated in previous work[6] and the surface kinetics used to treat oxide gasification in B/H/O/C environments.[5] The latter model has been extended to include heterogeneous reactions involving fluorine containing species. A series of calculations have been performed to characterize the droplets burning rate on its size and the temperature and composition of the surround gas. The model results suggest that fluorine can have an important impact promoting oxide gasification.

The addition of fluorine to the gas phase mixture surrounding a gasifying liquid B_2O_3 droplet at high temperatures has been predicted to increase the rate of gasification. For the conditions of the present study, the increase in the gasification rate ranged from 40% to a factor of 3.

For the conditions important to boron particle combustion, gasification of liquid B_2O_3 by surface reactions was predicted to always play an important role. The most sensitive surface reaction was found to be adsorption of HF except for highly fluorinated mixtures (F/O > 2) where F atom adsorption was the most sensitive reaction and for mixtures with small quantities of fluorine (F/O < 0.2) where H_2O adsorption became important. Adsorption steps were found to be rate controlling for all conditions studied except at the lowest temperature (1600 K) where desorption became the rate limiting process. Thus, the assumptions of considering only reactions first order in gas pasha reactants was found to be appropriate for this study.

The results also indicate that gasification will be kinetically controlled for particle diameters relevant to boron combustion. Transition of the gasification rate from a purely kinetically controlled process to one controlled totally by diffusion was found to occur over a wide range of diameters. Also, boundary layer effects were found to be significant for an initial particle diameter greater than 500μm. The implications of these results, particularly with regard to their transient behavior, are important to the interpretation of particle experimental data.

Recently, experimental studies of the interaction between HF and small boron oxide cluster ions have become available.[24] One interesting result of this data is the suggestion that formation of an BHOF surface complex may be an important adsorption channel. The significance on this data is currently being investigated and will be subsequently be incorporated into the model.

7.0 REFERENCES

1. Yetter, R.A., S.Y. Cho, H. Rabitz, Dryer, F.L., Brown, R.C. and Kolb, C.E., "Chemical Kinetic Modeling with Sensitivity Analyses for Boron Assisted Hydrocarbon Combustion," Twenty Second Symposium (International) on Combustion, p. 919, The Combustion Institute (1988).

2. Yetter, R.A., Rabitz, H., Dryer, F.L., Brown, R.C. and Kolb, C.E., Combustion and Flame 83, 43 (1991).

3. Brown, R.C., Kolb, C.E., Cho., S.Y., Yetter, R.A., Rabitz, H. and Dryer, F.L., in *Gas-Phase Metal Reactions*, (A. Fontijn, Editor,), Elsevier Science Publishers B.V., The Netherlands, 1992, p. 647

4. Brown, R.C., Kolb, C.E., Rabitz, H., Cho., S.Y., Yetter, R.A. and Dryer, F.L., Int. J. Chem. Kinetics 23, 957 (1991).

5. Brown, R.C., Kolb, C.E., Cho, S.Y., Yetter, R.A., Rabitz, H. and Dryer, F.L., "Kinetic Model for Hydrocarbon Assisted Particulate Boron Combustion," Int. J. Chem. Kinetics, in press , 1993.

6. Brown, R.C., Kolb, C.E., Yetter, R.A., Dryer, F.L., Rabitz, H., "Kinetic Modeling and Sensitivity Analysis for B/H/O/C/F Combustion Systems", submitted to Comb. Flame, 1993.

7. Cho, S.Y., Yetter, R.A., and Dryer, F.L., J. Comput. Physics, 1992.

8. Pasternak, L., Comb. and Flame 90, 259 (1992).

9. Page, M., J. Phys. Chem. 93, 3693, 1989.

10. Nguyen, M.T., Vanguickenborne, L.G., Sana, M. and Leroy, G., J. Phys. Chem. 97, 5224 (1993).

11. Hills, A.J. and Howard, C.J., J. Chem. Phys. 81, 4458 (1984).

12. JANNAF Thermochemical Tables, Third Edition, Parts I and II. J. Phys. and Chem. Ref. Data, V. 14 (1985).

13. Yetter, R.A., Dryer, F.L., and Rabitz, H.R., Combust. Sci. Tech. 79, 97 (1991).

14. DiGiuseppe, T.G. and Davidovits, P, J. Chem. 74, 3287 (1981).

15. DiGiuseppe, T.G., Estes, R. and Davidovits, P., J. Phys. Chem. 86, 260 (1982).

16. Llewellyn, I.P., Fontijn, A. and Clyne, M.A.A., Chem. Phys. Lett. 84, 504 (1981).

17. Oldenborg, R.C. and Baughcum, S.L., "Gas Phase Oxidation of Boron Compounds," Abstracts of the 1986 AFOSR/ONR Contractors Meeting on Combustion, pg. 57, June, 1986.

18. Oldenborg, R.C. and Baughcum, S.L., "Gas-Phase Oxidation of Atomic Boron and Boron Monoxide," in Advances in Laser Science-I, Proceedings of the First International Laser Science Conferences, Dallas, Tx, 1985.

19. Stanton, C. T. Garland, N.L., and Nelson, H.H., J. Phys. Chem. 95, 8741 (1991).

20. Garland, N.L., "Kinetic Studies of Boron and Aluminum Species," in Gas-Phase Metal Reactions, A. Fontijn, Editor, Elsevier Science Publishers B.V., The Netherlands, in press (1992).

21. Light, G.C., Herm, R.R. and Matsumoto, J.N., Chem. Phys. Lett. 89, 366 (1980).

22. Light, G.C., Herm, R.R. and Matsumoto, J.N., J. Phys. Chem. 89, 5066 (1985).

23.Wolfard, H.G., Draper, J.S., Riger, T.J., and Kolb, C.E., IDA, "Determination of the Infrared Emissions of Rocket Plumes and their Emitting Species," IDA paper P-1117, Institute for Defense Analysis, June, 1975.

24. Anderson, S., SUNY, Stony Brook, NY, private communication, 1993.

APPENDIX A. GAS PHASE REACTION MECHANISM

Table 15. B/O/H/C/F Reaction Mechanism

No.	Reaction	A	n_f	$E_{a,f}$
G-1	B+F+M=BF+M	$0.500 \times 10^{+16}$	0.0	-1987.0
G-2	BO+F+M=OBF+M	$0.364 \times 10^{+15}$	0.0	-1987.0
G-3	BF+O+M=OBF+M	$0.363 \times 10^{+15}$	-0.5	30.0
G-4	F+H+M=HF+M	$0.221 \times 10^{+23}$	-2.0	0.0
G-5	BF+F+M=BF_2+M	$0.363 \times 10^{+15}$	-0.5	-5961.0
G-6	BO_2+F=OBF+O	$0.120 \times 10^{+15}$	0.0	0.0
G-7	B_2O_2+F=OBF+BO	$0.241 \times 10^{+15}$	0.0	0.0
G-8	B_2O_3+F=OBF+BO_2	$0.241 \times 10^{+15}$	0.0	0.0
G-9	HBO+F=OBF+H	$0.108 \times 10^{+15}$	0.0	0.0
G-10	HBO+F=HF+BO	$0.361 \times 10^{+14}$	0.0	0.0
G-11	HBO_2+F=HF+BO_2	$0.361 \times 10^{+14}$	0.0	993.5
G-12	HBO_2+F=OBF+OH	$0.108 \times 10^{+15}$	0.0	0.0
G-13	B+HF=H+BF	$0.361 \times 10^{+15}$	0.0	0.0
G-14	BO+HF=OBF+H	$0.181 \times 10^{+13}$	0.0	6955.0
G-15	BO_2+HF=OBF+OH	$0.181 \times 10^{+12}$	0.0	9935.0
G-16	B_2O_2+HF=OBF+HBO	$0.313 \times 10^{+10}$	0.0	9935.0
G-17	B_2O_3+HF=OBF+HBO_2	$0.602 \times 10^{+9}$	0.0	11922.0
G-18	HBO+HF=OBF+H_2	$0.181 \times 10^{+12}$	0.0	9935.0
G-19	HBO_2+HF=OBF+H_2O	$0.157 \times 10^{+11}$	0.0	9935.0
G-20	BO_2+BF=OBF+BO	$0.301 \times 10^{+14}$	0.0	1987.0
G-21	BO+BF_2=OBF+BF	$0.602 \times 10^{+13}$	0.0	0.0
G-22	BO_2+BF_2=2OBF	$0.181 \times 10^{+12}$	0.0	9935.0
G-23	B+OBF=BO+BF	$0.422 \times 10^{+11}$	0.0	0.0
G-24	BF+O=BO+F	$0.843 \times 10^{+14}$	0.0	0.0
G-25	BF_2+O=OBF+F	$0.120 \times 10^{+15}$	0.0	0.0
G-26	BF_2+H=BF+HF	$0.301 \times 10^{+14}$	0.0	0.0
G-27	F+OH=HF+O	$0.301 \times 10^{+14}$	0.0	397.4
G-28	BF+OH=OBF+H	$0.120 \times 10^{+14}$	0.0	0.0
G-29	BF+OH=BO+HF	$0.602 \times 10^{+12}$	0.0	4968.0
G-30	BF_2+OH=OBF+HF	$0.181 \times 10^{+13}$	0.0	4968.0
G-31	BF+O_2=OBF+O	$0.108 \times 10^{+14}$	0.0	14390.0
G-32	F+H_2=HF+H	$0.163 \times 10^{+15}$	0.0	1590.0
G-33	F+H_2O=OH+HF	$0.602 \times 10^{+14}$	0.0	1987.0
G-34	BF_2+B=2BF	$0.361 \times 10^{+14}$	0.0	0.0
G-35	BF_2+HF=BF_3+H	$0.181 \times 10^{+13}$	0.0	9935.0
G-36	BF_3+B=BF_2+BF	$0.361 \times 10^{+14}$	0.0	0.0
G-37	2BF_2=BF_3+BF	$0.602 \times 10^{+12}$	0.0	0.0
G-38	BF_3+BO=BF_2+OBF	$0.602 \times 10^{+13}$	0.0	1987.0

Table 16. B/O/H/C Reaction Mechanism

No.	Reaction	A	n_f	$E_{a,f}$
G-39	$B+O_2=BO+O$	0.717×10^{14}	0.0	313.9
G-40	$B+O+M=BO+M$	0.110×10^{16}	0.0	-1987.0
G-41	$BO+O_2=BO_2+O$	0.421×10^{13}	0.0	-507.0
G-42	$BO+O+M=BO_2+M$	0.109×10^{16}	0.0	-1987.0
G-43	$B+BO_2=2BO$	0.361×10^{14}	0.0	0.0
G-44	$BO+BO_2+M=B_2O_3+M$	0.181×10^{14}	0.0	-1987.0
G-45	$2BO_2=B_2O_3+O$	0.602×10^{11}	0.0	9935.0
G-46	$B+OH=BO+H$	0.602×10^{14}	0.0	0.0
G-47	$BO+OH=BO_2+H$	0.241×10^{13}	0.0	0.0
G-48	$BO+OH+M=HBO_2+M$	0.363×10^{15}	0.0	-1987.0
G-49	$BO+H_2O=HBO_2+H$	0.602×10^{11}	0.0	9935.0
G-50	$BO_2+OH=HBO_2+O$	0.181×10^{13}	0.0	993.5
G-51	$BO_2+H+M=HBO_2+M$	0.181×10^{16}	0.0	-1987.0
G-52	$BO_2+H_2=HBO_2+H$	0.181×10^{13}	0.0	2981.0
G-53	$HBO_2+OH=BO_2+H_2O$	0.120×10^{13}	0.0	1987.0
G-54	$B_2O_3+H_2O=2HBO_2$	0.602×10^{9}	0.0	11922.0
G-55	$BO+H+M=HBO+M$	0.109×10^{16}	0.0	-1987.0
G-56	$BO+H_2=HBO+H$	0.452×10^{2}	3.53	3160.0
G-57	$BO+OH=HBO+O$	0.164×10^{4}	2.76	5015.0
G-58	$HBO+O=BO_2+H$	0.482×10^{14}	0.0	0.0
G-59	$HBO+OH=BO+H_2O$	0.482×10^{14}	0.0	0.0
G-60	$HBO+OH=HBO_2+H$	0.482×10^{14}	0.0	0.0
G-61	$HBO+OH=BO_2+H_2$	0.602×10^{4}	0.0	69942.0
G-62	$HBO+O_2=BO_2+OH$	0.602×10^{4}	0.0	69942.0
G-63	$HBO+O+M=HBO_2+M$	0.363×10^{21}	-0.5	50072.0
G-64	$2BO+M=B_2O_2+M$	0.363×10^{14}	0.0	-1987.0
G-65	$B_2O_2+H=BO+HBO$	0.602×10^{13}	0.0	0.0
G-66	$B_2O_2+O=BO+BO_2$	0.361×10^{14}	0.0	0.0
G-67	$B_2O_2+OH=BO+HBO_2$	0.361×10^{14}	0.0	0.0
G-68	$B_2O_2+OH=BO_2+HBO$	0.602×10^{4}	0.0	69942.0
G-69	$B_2O_2+O_2=2BO_2$	0.602×10^{4}	0.0	80076.0
G-70	$BO_2+CO=BO+CO_2$	0.301×10^{14}	0.0	1987.0
G-71	$B+H_2O=HBO+H$	0.241×10^{15}	0.0	2682.0
G-72	$B+CO_2=BO+CO$	0.422×10^{11}	0.0	0.0
G-73	$HBO+BO_2=HBO_2+BO$	0.182×10^{13}	0.0	990.0
G-74	$BO_2+HBO=B_2O_3+H$	0.182×10^{13}	0.0	990.0
G-75	$BO+HBO_2=B_2O_3+H$	0.482×10^{13}	0.0	0.0

Table 17. O/H/C Reaction Mechanism

No.	Reaction	A	n_f	$E_{a,f}$
G-76	$H+O_2=O+OH$	0.192×10^{15}	0.0	16440.0
G-77	$O+H_2=H+OH$	0.508×10^{5}	2.67	6292.0
G-78	$OH+H_2=H+H_2O$	0.216×10^{9}	1.51	3430.0
G-79	$2OH=O+H_2O$	0.123×10^{5}	2.62	-1878.0
G-80	$H_2+M=2H+M$	0.457×10^{20}	-1.4	104400.0
G-81	$2O+M=O_2+M$	0.617×10^{16}	-0.5	0.0
G-82	$O+H+M=OH+M$	0.472×10^{19}	-1.0	0.0
G-83	$H+OH+M=H_2O+M$	0.225×10^{23}	-2.0	0.0
G-84	$H+O_2+M=HO_2+M$	0.617×10^{20}	-1.42	0.0
G-85	$HO_2+H=H_2+O_2$	0.663×10^{14}	0.0	2126.0
G-86	$HO_2+H=2OH$	0.169×10^{15}	0.0	874.0
G-87	$HO_2+O=OH+O_2$	0.181×10^{14}	0.0	-397.0
G-88	$HO_2+OH=H_2O+O_2$	0.145×10^{17}	-1.0	0.0
G-89	$2HO_2=H_2O_2+O_2$	0.302×10^{13}	0.0	1390.0
G-90	$H_2O_2+M=2OH+M$	0.120×10^{18}	0.0	45500.0
G-91	$H_2O_2+H=H_2O+OH$	0.100×10^{14}	0.0	3590.0
G-92	$H_2O_2+H=H_2+HO_2$	0.482×10^{14}	0.0	7948.0
G-93	$H_2O_2+O=OH+HO_2$	0.955×10^{7}	2.0	3970.0
G-94	$H_2O_2+OH=H_2O+HO_2$	0.700×10^{13}	0.0	1430.0
G-95	$CO+O+M=CO_2+M$	0.251×10^{14}	0.0	-4541.0
G-96	$CO+O_2=CO_2+O$	0.253×10^{13}	0.0	47690.0
G-97	$CO+OH=CO_2+H$	0.150×10^{8}	1.3	-765.0
G-98	$CO+HO_2=CO_2+OH$	0.602×10^{14}	0.0	22950.0
G-99	$HCO+M=H+CO+M$	0.186×10^{18}	-1.0	17000.0
G-100	$HCO+O_2=CO+HO_2$	0.758×10^{13}	0.0	410.0
G-101	$HCO+H=CO+H_2$	0.723×10^{14}	0.0	0.0
G-102	$HCO+O=CO+OH$	0.302×10^{14}	0.0	0.0
G-103	$HCO+OH=CO+H_2O$	0.302×10^{14}	0.0	0.0

APPENDIX B. B(s) SURFACE OXIDATION MECHANISM

B-1. Global Reactions

Global reactions for particulate boron surface oxidation in B/H/O/C/F combustion systems are listed in Table 18. These reactions were selected using three criteria: (1) reactions first order in gas phase reactants (2) reactions whose reaction enthalpy is less than 150 Kcal/mol (3) reactions yielding gas phase products which are consistent with the B/H/O/C/F gas phase oxidation model. Reactions R_1-R_{15} are the surface reactions previously used to treat B/H/O/C systems. Reactions R_{16}-R_{20} are the new surface reactions which arise when fluorine is added to the system.

Table 18. Global Reactions B(s) + Z(g) = Products

Reaction	ΔH_f(Kcal/mol)
R_1 B(s) + O(g) = BO(g)	-59.6
R_2 B(s) + O_2(g) = BO_2(g)	-68.0
R_3 B(s) + O_2(g) = BO(g) + O(g)	59.6
R_4 2B(s) + O_2(g) = B_2O_2(g)	-109.0
R_5 2B(s) + O_2(g) = 2BO(g)	0.0
R_6 B(s) + OH(g) = HBO(g)	-56.7
R_7 B(s) + OH(g) = BO(g) + H(g)	42.8
R_8 B(s) + H_2O(g) = BO(g) + H_2(g)	57.8
R_9 B(s) + H_2O(g) = HBO(g) + H(g)	.5
R_{10} B(s) + BO_2(g) = B_2O_2(g)	-41.0
R_{11} B(s) + BO_2(g) = 2BO(g)	68.0
R_{12} B(s) + B_2O_3(g) = B_2O_2(g) + BO(g)	90.8
R_{13} B(s) + HOBO(g) = BO(g) + HBO(g)	86.6
R_{14} B(s) + HOBO(g) = B_2O_2(g) + H(g)	77.1
R_{15} B(s) + CO_2(g) = BO(g) + CO(g)	67.7
R_{16} B(s) + F(g) = BF(g)	-46.7
R_{17} B(s) + HF(g) = BF(g) + H(g)	89.5
R_{18} B(s) + BF_2(g) = BF(g) + BF(g)	85.6
R_{19} B(s) + BF_3(g) = BF(g) + BF_2(g)	102.7
R_{20} B(s) + OBF(g) = BO(g) + BF(g)	116.3

B-2. Adsorption and Desorption Channels

Surface speciation is listed in Table 20 and first-order adsorption rate paramters are given in Table 21. The adsorption enthalpies are expresses in terms of the heats of formation given in Table 20 for the surface complexes. First-order desorption channels and rate parameters are listed in Table 22.

Table 20. B(s) Surface Species - Estimated Heats of Formation

Complex	Heat of Formation (Kcal/mol)
C_1 BO(c)	-71.0
C_2 BH(c)	26.0
C_3 HBO(c)	-45.0
C_4 BCO(c)	-80.0
C_5 B_2O_2(c)	-70.0
C_6 BF(c)	-45.0

Table 21. First-order Adsorption Rate Parameters for Boron Surface*

Adsoprtion Reaction	ΔH_a (Kcal/mol)	K_a (cm/s)	s_0	E_a (cal/mol)
S-1 B(s) + H = BH(c)	H_2-52.1	3623	0.1	0.0
S-2 B(s) + O = BO(c)	H_1-59.6	909	0.8	0.0
S-3 2B(s) + O_2(g) = B_2O_2(c)	-109.0	643	0.064	1014.0
S-4 2B(s) + O_2(g) = BO(c) + BO(g)	H_1	643	0.0082	0.0
S-5 B(s) + O_2(g) = BO(c) + O(g)	H_1+59.6	643	0.001	1000.0
S-6 B(s) + OH(g) = BO(c) + H(g)	H_1-42.8	882	0.02	1000.0
S-7 B(s) + OH(g) = HBO(c)	H_3-0.3	882	0.02	1000.0
S-8 B(S) + H_2O(g) = BH(c) + HBO(g)	H_2-2.2	857	0.0062	8000.0
S-9 B(s) + BO_2(g) = B_2O_2(c)	H_5+68.0	556	0.005	5000.0
S-10 B(s) + BO_2(g) = BO(c) + BO(g)	H_1+68.0	556	0.005	5000.0
S-11 B(s) + B_2O_3(g) = B_2O_2(g) + BO(g)	90.8	436	0.87	0.0
S-12 B(s) + HOBO(g) = HBO(c) + BO(g)	H_2+134.0	549	0.0025	4000.0
S-13 B(s) + HOBO(g) = B_2O_2(c) + H(g)	H_5+186.1	549	0.0025	4000.0
S-14 B(s) + CO_2(g) = BO(c) + CO(g)	H_1+67.7	548	0.0013	4517.0
S-15 B(s) + CO(g) = BCO(c)	H_4+26.5	687	0.00015	0.0
S-16 B(s) + BO(g) = B_2O(c) ≡ BO(c)	H_1	reverse of BO(c) desorption		
S-17 B(s) + B_2O_2(g) = B_3O_2(c) ≡ B_2O_2(c)	H_5+109.0	reverse of B2O2(c) desorption		
S-18 B(s) + HBO(g) = HB_2O(c) ≡ HBO(c)	H_3+60.0	reverse of HBO(c) desorption		
S-19 B(s) + F(g) = BF(c)	H_6	882	0.02	1000.0
S-20 B(s) + HF(g) = BF(c) + H(g)	H_6+52.1	857	0.0062	10,000.0
S-21 2B(s) + HF(g) = BH(c) + BF(c)	H_6+H_2	857	0.0062	10,000.0
S-22 B(s) + BF_2(g) = BF(c) + BF(g)	H_6-27.7	900	0.004	3000.0
S-23 B(s) + BF_3(g) = BF(c) + BF_2(g)	H_6-141.0	900	0.004	3000.0
S-24 B(s) + OBF(g) = BF(c) + BO(g)	H_6	549	0.0025	4000.0
S-25 B(s) + BF(g) = BF(c)	H_6	reverse of BF(c) desorption		

* H_i represents the heat of formation for surface species C_i

Table 22. B(s) Surface - Desorption Rate Parameters*

Complex	Desorption Channels	ΔH_I (Kcal/mol)	A_I (ps-1)	E_I (Kcal/mol)
BH(c)	B(s) + H(g)	52.1-H_2	reverse S-1	
BO(c)	BO(g)	-H1	0.02xT	-H1
	B(s) + O(g)	59.6-H1	reverse S-2	
B2O2	B_2O_2(g)	-109.0-H_5	0.02xT	-109.0-H_5
	2B(s) + O_2(g)	-68.0-H_5	reverse S-3	
HBO(c)	HBO(g)	-60.0-H_3	0.02xT	-60.0-H_3
	BO(g) + H(g)	52.1-H_3	0.02xT	52.1-H_3
	B(s) + OH(g)	9.3-H_3	reverse S-7	
BCO(c)	B(s) + CO(g)	-26.4-H_4	reverse S-15	
BF(c)	BF(g)	-H_6	0.02xT	-H_6
	B(s) + F(g)	18.97-H_6	reverse S-19	

* H_i represents the heat of formation for surface species C_i